Journal of Sedimentary Research, 2025, v. 95, 760–776
Research Article
DOI: 10.2110/jsr.2024.005

UNROOFING AND PROVENANCE OF THE MIOCENE AUSTRAL–MAGALLANES FORELAND BASIN, ARGENTINA

INÉS ARAMENDÍA,[1,2] JOSÉ IGNACIO CUITIÑO,[1] MARÍA SOL RAIGEMBORN,[3,4] PABLO BOUZA,[1]
JUAN VRDOLJAK,[5,6] AND MATÍAS C. GHIGLIONE[7,8]
[1]*Instituto Patagónico de Geología y Paleontología, Boulevard Brown 2915, Puerto Madryn, Chubut, Argentina*
[2]*Department of Earth Sciences, University of Geneva, Rue des Maraîchers 13, 1205 Geneva, Switzerland*
[3]*Centro de Investigaciones Geológicas, Diagonal 113 no. 275, La Plata, Buenos Aires, Argentina*
[4]*Facultad de Ciencias Naturales y Museo, Calle 122 s/n, La Plata, Buenos Aires, Argentina*
[5]*Instituto Patagónico para el Estudio de Ecosistemas Continentales, Boulevard Brown 2915, Puerto Madryn, Chubut, Argentina*
[6]*Universidad Nacional de la Patagonia San Juan Bosco, Boulevard Almirante Brown 3051, U9120ACD Puerto Madryn, Chubut, Argentina*
[7]*Instituto de Estudios Andinos "Don Pablo Groeber," Intendente Güiraldes 2160, Ciudad Universitaria–Pabellón II, Buenos Aires, Argentina*
[8]*Departamento de Ciencias Geológicas, Universidad de Buenos Aires, Intendente Güiraldes 2160, Ciudad Universitaria–Pabellón II, Buenos Aires, Argentina*
e-mail: ines.aramendia91@gmail.com

ABSTRACT: **Provenance studies are widely used in foreland basin settings to evaluate temporal changes in sediment source areas, pinpoint the composition of outcropping units during deposition, and shed light on the interactions between source-area composition, depositional environments, tectonics, and paleoclimate. We present a case example from the Miocene foreland basin of the Austral–Magallanes in southern Patagonia, Argentina (46.5–47.9° south latitude), providing provenance studies of conglomerates, sandstones, and mudstones, combined with previously published detrital-zircon U–Pb geochronology and sedimentological data. Based on this information, we document a change in volcaniclastic source areas consistent with an unroofing sequence during the main phase of Andean tectonic uplift. The studied Miocene beds are up to 1000 m thick and represent a synorogenic environmental transition from shallow marine (El Chacay Formation, ∼ 20–18 Ma) to fluvial–alluvial (Río Zeballos Group, ∼ 18–12 Ma), and ultimately to fluvial (Santa Cruz Formation, ∼ 18–14 Ma) paleoenvironments. Litharenite and feldspathic litharenite thin-section samples ($n = 51$) plot within the magmatic-arc and recycled-orogen tectonic fields. Six conglomerate samples indicate a similar setting. Furthermore, X-ray diffraction analysis of 36 mudstone samples identifies a well-crystallized smectite clay mineral, commonly associated with illite, mixed-layer illite–smectite, chlorite, minor calcite, and zeolites, suggesting the alteration of labile volcanic material from orogenic sources. Our compositional evidence, together with previous detrital U–Pb zircon data, characterizes the studied unroofing sequence exposing Mesozoic to Paleozoic rocks, and serves as a case study for other orogenic basins, where the progressive tectonic exhumation of source areas plays a dominant role.**

INTRODUCTION

Foreland basins are elongated areas that develop on continental crust through lithospheric flexure in the retroarc region associated with mountain ranges (DeCelles and Giles 1996; Allen and Allen 2005; Horton 2018). These active sedimentary basins and their stratigraphic architecture are influenced by, and record, tectonic, provenance, and climate changes (e.g., Jervey 1988; Vaucher et al. 2024). A useful tool for identifying potential source areas and understanding the relationship between shifts in compositional frameworks and changes in orogenic-wedge behavior in sedimentary basins is the modal composition of sandstones and conglomerates (Ingersoll 1983; Cavazza 1989; Howard 1993; Garzanti et al. 2007; Caracciolo et al. 2011; Spalletti et al. 2012; Ciccioli et al. 2014; Sickmann et al. 2019; Leonard et al. 2020; Critelli and Criniti 2021). Sedimentary provenance studies allow us to track unroofing sequences in foreland basins over geologic timescales (Horton et al. 2004; Leonard et al. 2020; Critelli and Criniti 2021).

The most widely accepted unroofing model, proposed by Allen and Allen (2005), is based on two premises: i) the provenance imprint is characterized by sediments that are close in age and deposited contemporaneously with sedimentary units, supplying material to the basin infill; and ii) as the orogen grows, exhumation exposes older lithological units, subsequently providing sediment to the basin. Critelli and Criniti (2021) proposed a logical evolution of an unroofing event in ancient foreland basins based on sandstone petrography. The authors identified three types of sandstone signatures: i) a quartz-rich provenance from the underplate flanks, ii) a variable provenance from the fold-and-thrust belt, where an unroofing sequence is expected, and iii) a predictable evolution marked by an increase in feldspar and lithic fragments from the deeper lithological units exposing the orogenic roots. This study examines the evolution of sediment provenance in a foreland-basin infill to explore its response to tectonic reconfiguration in the surrounding geodynamic setting. Using three complementary methodologies applied to sandstones, conglomerates, and mudstones, we aim to identify an unroofing

Published Online: August 2025
Copyright © 2025, SEPM (Society for Sedimentary Geology) 1527-1404/25/095-760

Downloaded from http://pubs.geoscienceworld.org/sepm/jsedres/article-pdf/95/4/760/7321069/10.2110_jsr.2024.005.pdf
by Universidad Nacional de La Plata user

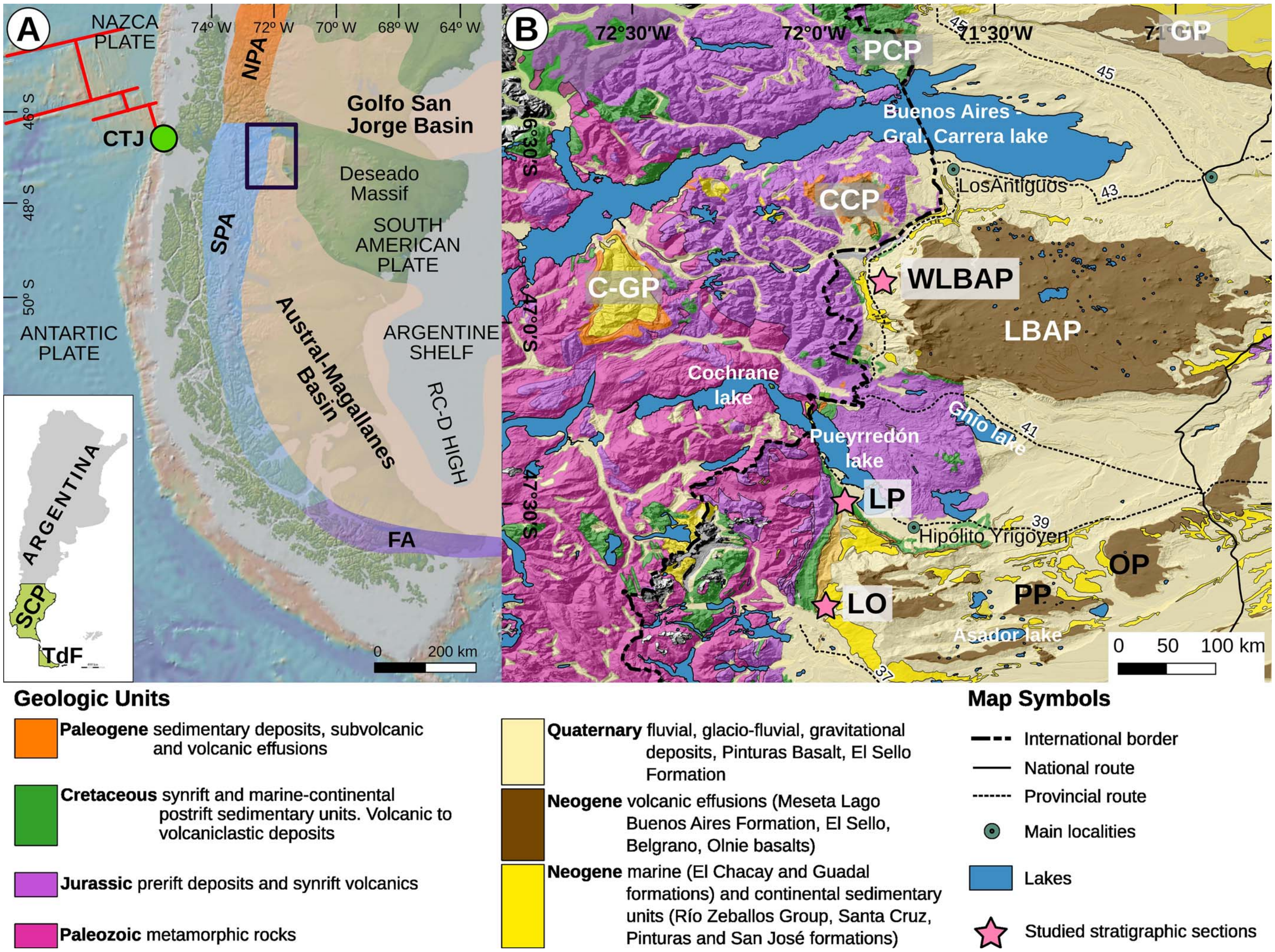

FIG. 1.—Location of the study area. **A)** Geographic and morphostructural limits of the Austral–Magallanes Basin mentioned in the text. The green point shows the present-day location of the Chile Triple Junction (CTJ). NPA, Northern Patagonian Andes; SPA, Southern Patagonian Andes; FA, Fueguian Andes; RC-D, Río Chico–Dúngenes High; SCP, Santa Cruz province; TdF, Tierra del Fuego province. Black rectangle represents the study area. Global Multi-Resolution Topography base map from GeoMapApp©. **B)** Detailed geologic map of the study region showing the location of the main Miocene outcrops and volcanic and sedimentary plateaus. Pink stars highlight the location of the three stratigraphic sections sampled for this work: WLBAP, western Lago Buenos Aires Plateau; LP, Lago Posadas; LO, La Oriental; PCP, Pampa Castillo Plateau; GP, Guenguel Plateau; CCP, Chile Chico Plateau; C-GP, Cosmelli–Guadal Plateau; LBAP, Lago Buenos Aires Plateau; PP, Pobre Plateau; OP, Olnie Plateau. Modified from Aramendía et al. (2019, 2022).

sequence in the Miocene foreland basin of the Austral–Magallanes Basin, located at the foothills of the Southern Patagonian Andes. These Miocene strata, up to 1000 m thick, span the basin's northwestern margin between Lago Buenos Aires and Lago Belgrano (46.5–47.9° S latitude) and include the shallow marine El Chacay Formation, the fluvial–alluvial Río Zeballos Group, and the fluvial Santa Cruz Formation (Aramendía et al. 2019, 2022).

Our findings constrain sediment sources and confirm a previously documented unroofing sequence, highlighting sedimentary and tectonic processes associated with late Miocene Andean uplift. By integrating provenance data from this study with published sandstone analyses (Barberón et al. 2019; Cuitiño et al. 2019a) and detrital-zircon records (Aramendía et al. 2022), we evaluate how each methodology elucidates the unroofing sequence and contributes to understanding foreland-basin evolution. This research provides valuable insights into the transition from shallow marine (~ 20–18 Ma) to fluvial–alluvial deposits (~ 18–12 Ma), enhancing our knowledge of regional uplift, magmatic evolution, and foreland-basin dynamics within a broader tectonic framework.

GEOLOGICAL SETTING

Stratigraphic Succession

The Austral–Magallanes Basin is located on the retroarc of the southernmost Andes, partially covering the Santa Cruz and Tierra del Fuego provinces, and extending offshore onto the Argentine shelf (Fig. 1A). The morphostructural boundaries of the basin include tectonically active zones such as the Southern Patagonian Andes (SPA) to the west and the Fueguian Andes to the south, which are potential sources of sediment and active volcanism, along with the cratonic Deseado Massif to the northeast (Fig. 1A). The Austral–Magallanes and offshore Malvinas basins are connected through a continuous depocenter running along the southern boundary of the South American Plate. However, they are separated to the north by the Río Chico–Dúngenes basement high (Ghiglione et al. 2010).

In the study area, the basin rests atop Devonian to Carboniferous metasedimentary basement composed of strongly deformed, low-grade-metamorphosed turbiditic beds of the Río Lácteo Formation (Hervé et al. 2008;

Downloaded from http://pubs.geoscienceworld.org/sepm/jsedres/article-pdf/95/4/760/7321069/10.2110_jsr.2024.005.pdf
by Universidad Nacional de La Plata user

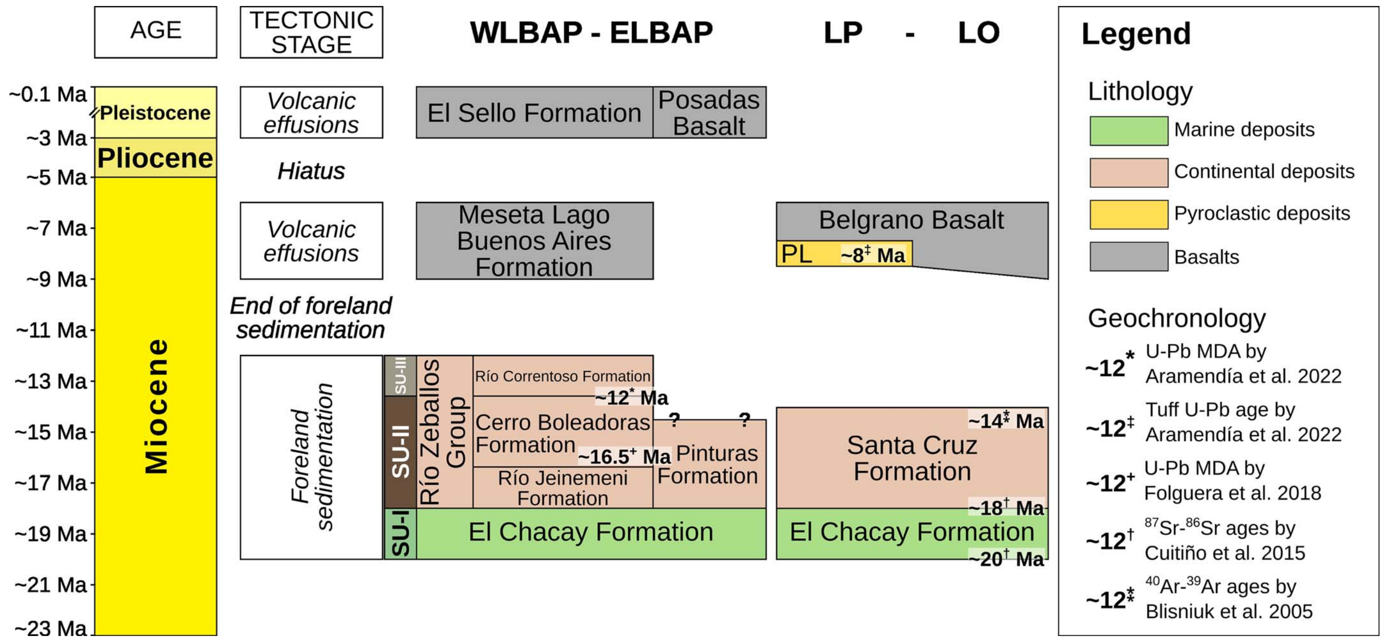

FIG. 2.—Stratigraphic chart for the study area with the previous published age constrained for the Miocene sedimentary infill of the northwestern edge of the Austral–Magallanes basin. ELBAP, eastern Lago Buenos Aires Plateau; SU, sedimentary unit; PL, pyroclastic level; MDA, maximum depositional age. Modified from Aramendía et al. (2019).

Escosteguy et al. 2017). Jurassic syn-rift successions unconformably overlie this basement, beginning with coalescent alluvial fans and sheet-flood deposits of the El Bello Formation (Fig. 1B). These deposits grade upward into widely distributed volcanic and volcano-sedimentary successions of the El Quemado Complex, representing the main phase of mechanical rifting (Giacosa et al. 2001; Escosteguy et al. 2003, 2017).

Lower Cretaceous thermal sag deposits are represented by continental to shallow marine deposits of the Springhill (Berriasian–Valanginian) and open marine Río Mayer (Hauterivian–Barremian) formations (Aguirre-Urreta and Ramos 1981; Richiano et al. 2012, 2015, 2016). These are overlain by Aptian–Cenomanian early foreland deposits of the deltaic Río Belgrano Formation and subsequent volcaniclastic fluvial deposits of the Río Tarde, Kachaike, and Cardiel formations (Ghiglione et al. 2015; Aramendía et al. 2018; Cuitiño et al. 2019b) (Fig. 1B). Upper Paleocene–lower Eocene fluvial quartz-rich deposits of the Ligorio Márquez Formation and the mudstone-dominated beds containing fossil wood and leaf remains of the Río Lista Formation cover the Mesozoic units in the study area (Escosteguy et al. 2001, 2003; Encinas et al. 2019) (Fig. 1B). Widespread Eocene basaltic volcanic beds in the area include the Posadas Basalt (Escosteguy et al. 2003) and minor subvolcanic intrusions (Fig. 1B).

Above a regional unconformity, the Neogene synorogenic succession begins with the marine Patagoniense deposits, representing an Atlantic marine transgression widespread in Patagonia during the early Miocene (Malumián and Náñez 2011; Encinas et al. 2019; Parras and Cuitiño 2021) (Figs. 1B, 2). In the study area, these marine deposits are assigned to the El Chacay Formation, following Parras et al. (2012), Cuitiño et al. (2015, 2019a, 2019b), and Aramendía et al. (2019, 2022). The age of these beds is constrained to 22–18 Ma based on $^{87}Sr/^{86}Sr$ isotope ratios in oysters and U–Pb detrital-zircon analysis (Cuitiño et al. 2012; Parras et al. 2012; Cuitiño et al. 2015). Transitionally overlying the El Chacay Formation, fluvial to alluvial-fan deposits are recognized in the area (Aramendía et al. 2019, 2022). Along the western and southern borders of the Lago Buenos Aires Plateau, these beds were defined as the Río Zeballos Group by Ugarte (1956). This group includes the Río Jeinemeni, Cerro Boleadoras, and Río Correntoso formations, with an age constrained between ~ 18 and ~ 12 Ma, representing the youngest Miocene clastic wedge in the basin (Aramendía et al. 2022) (Fig. 2). In the southern part of the study area, the equivalent Miocene fluvial deposits are referred to as the Santa Cruz Formation (Feruglio 1949; Furque 1973; Cuitiño et al. 2019b) or the Pinturas Formation along the eastern slope of the Lago Buenos Aires Plateau (De Barrio et al. 1984; Bown and Larriestra 1990) (Fig. 2). Near Lago Posadas, the Santa Cruz Formation's age has been constrained to 22–14 Ma based on $^{40}Ar/^{39}Ar$ dating of tuffaceous deposits (Blisniuk et al. 2005). Ages for the Río Zeballos Group suggest that sedimentation and compressional tectonics ceased between 14 and 12 Ma, with sediment bypassing to other depositional areas (Lagabrielle et al. 2004; Scalabrino et al. 2009; Aramendía et al. 2022).

The top of the Río Zeballos Group is principally covered by late Miocene–Quaternary basalts of the Meseta Lago Buenos Aires Formation (Gorring et al. 1997; Ton-That et al. 1999; Kay et al. 2002), dated from 9 Ma to 0.2 Ma (Sinito 1980; Ramos and Kay 1992; Aramendía et al. 2022) (Fig. 2). The Santa Cruz Formation is overlain by the Belgrano Basalt, which is no older than late Miocene, based on its correlation with the Strobel Basalt dated to 9–6 Ma by $^{40}Ar/^{39}Ar$ (Ramos and Kay 1992). The age of the Belgrano Basalt is also constrained by a primary tuff lying just below it, with a zircon U–Pb age of 8 Ma (Aramendía et al. 2022).

Tectonic History

The study area is located in the present-day deformation front of the SPA, characterized by the tectonic inversion of Mesozoic rift structures and tectonic thrusts (Suárez 1976; Ramos 1989; Kraemer and Riccardi 1997; Lagabrielle et al. 2004; Ronda et al. 2019). This tectonic scenario produced localized growth strata and syntectonic unconformities within the Neogene succession (Barberón et al. 2018). Denudation along the eastern margin of the basement domain in the SPA, recorded in young apatite fission-track ages, range between 9 and 4 km with ages between 14 and 5 Ma (Fosdick et al. 2013) or 12 and 8 Ma (Thomson et al. 2001; 2010). However, low-temperature thermochronology reveals that the easternmost extent of contraction was reached between 20 and 10 Ma (i.e., synchronous with the deposition of the

Downloaded from http://pubs.geoscienceworld.org/sepm/jsedres/article-pdf/95/4/760/7321069/10.2110_jsr.2024.005.pdf
by Universidad Nacional de La Plata user

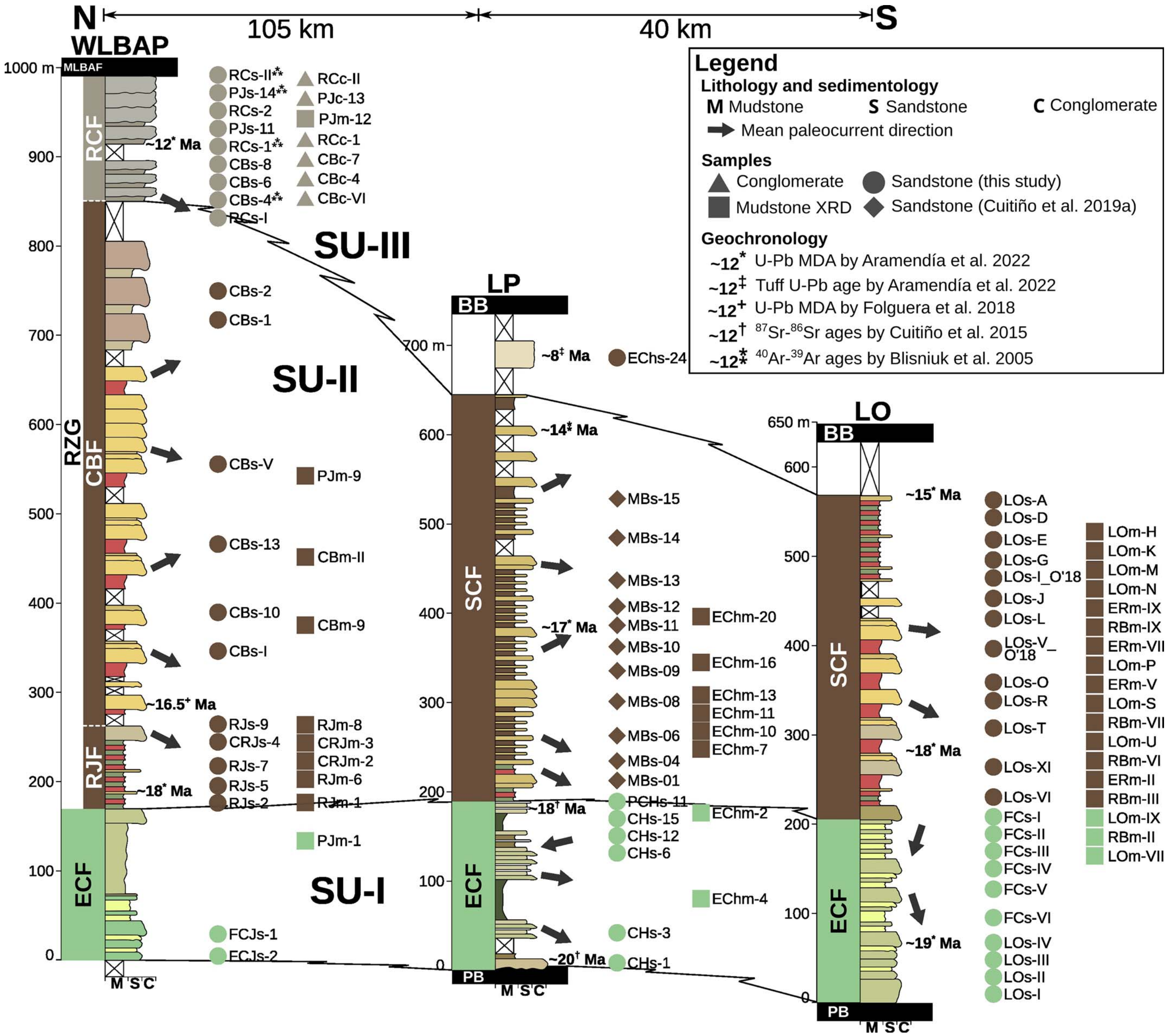

FIG. 3.—Sample distribution for the three stratigraphic sections in the study area. Main paleocurrent directions and previous published ages are highlighted. PB, Posadas Basalt; BB, Belgrano Basalt; MLBAF, Meseta Lago Buenos Aires Formation; ECF, El Chacay Formation; RZG, Río Zeballos Group; RJF, Río Jeinemeni Formation; CBF, Cerro Boleadoras Formation; RCF, Río Correntoso Formation; SCF, Santa Cruz Formation. Paleocurrent measured in the through cross-bedding beds, for SU-I n = 59, for SU-II n = 74, and for SU-III n = 10.

study sequences) and was followed by post 10 Ma glacial erosion-induced exhumation and contraction of deformation (Ronda et al. 2022).

MATERIALS AND METHODS

To characterize the composition and provenance of the Miocene succession we focus on three sections previously described and analyzed (Aramendía et al. 2019, 2022): Western Lago Buenos Aires Plateau (WLBAP), Lago Posadas (LP), and Laguna La Oriental (LO) (Figs. 1B, 3). Three sedimentary units (SUs) were defined for the entire Miocene succession: SU-I, shallow marine deposits (El Chacay Formation, ~ 20–18 Ma); SU-II, mixed-load fluvial deposits (Río Jeinemeni, Cerro Boleadoras, and Santa Cruz formations, ~ 18–14 Ma); and SU-III, alluvial fan deposits (Río Correntoso Formation, ~ 14–12 Ma; see Aramendía et al. 2022 for further description; Fig. 3). From the three stratigraphic sections six conglomerates were sampled for clast counting, 51 medium-grained sandstones for petrographic modal analysis, and 36 mudstones for X-ray diffraction (XRD) analysis (Fig. 3). Sandstone samples include the tabular marine sandstone bodies of the SU-I and the fluvial channel bodies every 30 m of section at SU-II, whereas mudstone samples come from the heterolithic deposits of SU-I, the fluvial floodplain beds from SU-II and SU-III with a vertical spacing of 30 to 40 m. Conglomerates are present only at the top of the WLBAP section (SU-III; Fig. 3), and samples are from gravel-dominated alluvial-fan channel bodies and frictional debris-flow deposits due to alluvial-fan growth.

Sandstone thin sections were subjected to standard petrographic analysis using a binocular Zeiss Axioplan microscope with a Nikon Coolpix 8400 for

Downloaded from http://pubs.geoscienceworld.org/sepm/jsedres/article-pdf/95/4/760/7321069/10.2110_jsr.2024.005.pdf
by Universidad Nacional de La Plata user

TABLE 1.—*Sandstone and conglomerate lithotypes.*

Code	Clast Description
	Sandstones
Qm	Monocristalline quartz
Qp	Polycrystalline quartz with three or more individuals
Plgz	Zoned plagioclase
Plgp	Polysynthetic-twins plagioclase
K	Potassium feldspar
Lsm	Fine-grained sedimentary fragment
Lss	Sandstone sedimentary fragment
Lml	Low-grade metamorphic fragment
Lmh	High-grade metamorphic fragment
Lvb	Mafic volcanic fragment with lathwork texture
Lva	Acidic volcanic fragment with microlithic to felsitic texture
Lpb	Mafic-composition plutonic fragment
Lpa	Acidic-composition plutonic fragment
Acc	Accessories including: clinopiroxene, clinoamphiboles, muscovite, biotite, undifferentiate opaque minerals, glauconite
Q	Total quartz grains: Qm + Qp
P	Total plagioclase grains: Plgz + Plgp
F	Total feldspar grains: P + K
L	Total lithic fragments: Lsp + Lsa + Lml + Lmh + Lvb + Lva + Lpb + Lpa
Lm	Total lithic metamorphic fragments: Lml + Lmh
Lv	Total lithic volcanic fragments: Lvb + Lva
Ls	Total sedimentary lithic fragments: Lsm + Lss
	Conglomerates
Q	Quartz
Ls	Sandstone sedimentary fragment
Lml	Low-grade metamorphic fragment
Lvb	Mafic-texture volcanic fragment
Lva	Acidic-texture volcanic fragment
Lsvb	Mafic volcanic fragment with subvolcanic texture
Lsva	Acidic volcanic fragment with subvolcanic texture
Lpa	Acidic plutonic fragment
Ltu	Tuffaceous lithic fragment

grain-type photomicrographs at the Instituto Patagónico de Geología y Paleontología, CCT CONICET-CENPAT, Chubut, Argentina. To discriminate between plagioclase feldspar, potassium feldspar, and quartz, samples were prepared with a saturated solution of sodium cobaltinitrite (Hutchinson 1974), which stains plagioclase grains red to pink and potassium feldspars yellow (Hutchinson 1974). In each sandstone sample, 450 grains were counted following the Gazzi-Dickinson method (Ingersoll et al. 1984) using a mechanical Swift Point counter at the Departamento de Geología, Facultad de Ciencias Exactas y Naturales, Universidad de Buenos Aires, Argentina. Sandstone framework elements of the samples are shown in Table 1 and some examples are depicted in Figure 4. Quartz (Q) grains were separated into monocrystalline (Qm) and polycrystalline (Qp) types. Among feldspars (F), potassium feldspar (K) and plagioclase (P) were recognized. Additionally, plagioclase-feldspar grains with zoning textures (Plgz) and plagioclase feldspars with polysynthetic albite twinning (Plgp) were counted separately. Lithic fragments (L) include volcanic (Lv), metamorphic (Lm), plutonic (Lp), and sedimentary (Ls) grains. Volcanic grains were subdivided according to their textures reflecting different magma compositions (e.g., Dickinson 1970; Critelli and Ingersoll 1995; Critelli et al. 2002): volcanic lithics with lathwork (Lvb) and felsitic to microlitic (Lva) textures. Metamorphic fragments (Lm) are separated into low grade (Lml) including phyllite and slates, and high grade (Lmh) (schists and amphibolites). Plutonic lithic fragments (Lp) are fine granular texture with plagioclase, muscovite, and quartz crystals. Sedimentary rock fragments (Ls) were categorized as mudstone (Lsm) and sandstone lithic fragments (Lss). Accessory minerals include micas (biotite and muscovite), clinoamphiboles, clinopyroxenes, opaques, and glauconite. The volume of porosity was determined optically following the criteria of Folk et al. (1970).

Modal composition of sandstone samples are classified according to the Q:F:L (quartz, feldspars, and rock fragments) ratio of Folk et al. (1970). The relation among these modal components, the presence of different kinds of feldspars, the relative amounts of volcanic, sedimentary, and metamorphic rock fragments, and the discrimination between different types of volcanic lithics, among other features, are the basis for inferring the sediment source (Dickinson and Suczek 1979; Ingersoll et al. 1984; Dickinson 1985; Ingersoll 1990; Critelli et al. 1997, 2002). Due to the limited dispersion of the studied samples when plotted on the traditional ternary diagrams of Dickinson et al. (1983), custom ternary diagrams were devised to better establish spatial-temporal trends for the study succession.

To complement the point-counting analysis conducted on the sandstone samples, a statistical study was performed to describe the variation in the primary grain types (*sensu* Folk et al. 1970) across the three stratigraphic sections and among the three sedimentary units, aiming to detect shifts in provenance. A linear model was fitted to the proportions of each main grain type using 10,000 random permutations of the data (Anderson 2001; Anderson and Braak 2003) through a randomized residual permutation procedure (Collyer et al. 2015). The explanatory variable was the interaction between sedimentary units (three statistical levels: I, II, and III) and sections (three statistical levels: WLBAP, LO, and LP). Since SU-III is present only in section WLBAP, the interaction term resulted in seven statistical levels: WLBAP-I, WLBAP-II, WLBAP-III, LO-I, LO-II, LP-I, and LP-II. Post hoc pairwise comparisons of means and variances between these statistical levels were conducted within the random permutation framework of the linear model (Collyer et al. 2015). All statistical analyses were performed in R (R Core Team, 2024, Version 4.4.1) using the RRPP package (Collyer and Adams 2018, 2024). Considering the arbitrary nature of p-value thresholds (Benjamin et al. 2017; Dushoff et al. 2019), p-values were interpreted as follows: $p < 0.001$ indicates very strong support for differences, $p < 0.01$ strong support, $p < 0.05$ moderate support, $p < 0.1$ weak support, and $p > 0.1$ no evidence for differences (for detailed p-values the reader is referred to Appendix D). The p-values were corrected by the Holm method (Holm 1979).

Mudstone samples were selected for XRD analysis of the powder bulk rock and the oriented aggregates of the clay fraction (< 2 μm). They were subjected to soft grinding with a rubber mortar and sieved through a 105 μm mesh for powder XRD, while the clay fraction was separated by using Stokes's Law ("pipette method") and oriented aggregate mounts were prepared on glass slides. Clay mineralogy was determined from diffraction patterns obtained using samples that were air-dried, ethylene glycol-solvated for 24 h, and heated to 550°C for 2 h (Brown and Brindley 1980). Diffractograms were run on an X PANanlytical model X'Pert PRO diffractometer at the Centro de Investigaciones Geológicas, CONICET–UNLP, La Plata, Argentina. Routine air-dried mounts were run between 2 and 32°2θ at scan speed of 2°2θ/min. Ethylene glycol-solvated and heated samples were run from 2 to 27°2θ and 3 to 15°2θ, respectively, at a scan speed of 2°2θ/min. Semiquantitative whole-rock estimates were obtained from the intensity of the main peak for each mineral following the peak-area method, and the diffraction intensities used were taken from Schultz (1964), Biscaye (1965), and Moore and Reynolds (1997). Semiquantitative estimates of the relative percentages of clay minerals were also based on the peak-area method (Biscaye 1965) on glycolated samples (001 for smectite, illite and mixed-layers illite–smectite; 002 for chlorite) by applying empirical factors (Moore and Reynolds 1997).

For each conglomerate sample the composition of 300–400 clasts ranging between pebbles (up to 5 cm) and cobbles (up to 25 cm) was determined weighting the mode according to the size of the clasts (Cavazza 1989; Howard 1993). Results were grouped into nine lithotypes (Table 1; Fig. 5): quartz (Q, Fig. 5A), sedimentary (Ls, Fig. 5B), low-grade metamorphic (Lml, Fig. 5C), mafic volcanic (Lvb, Fig. 5D), felsic volcanic (Lva, Fig. 5E), mafic sub-volcanic (Lsvb, Fig. 5F), felsic sub-volcanic (Lsva, Fig. 5G),

Downloaded from http://pubs.geoscienceworld.org/sepm/jsedres/article-pdf/95/4/760/7321069/10.2110_jsr.2024.005.pdf
by Universidad Nacional de La Plata user

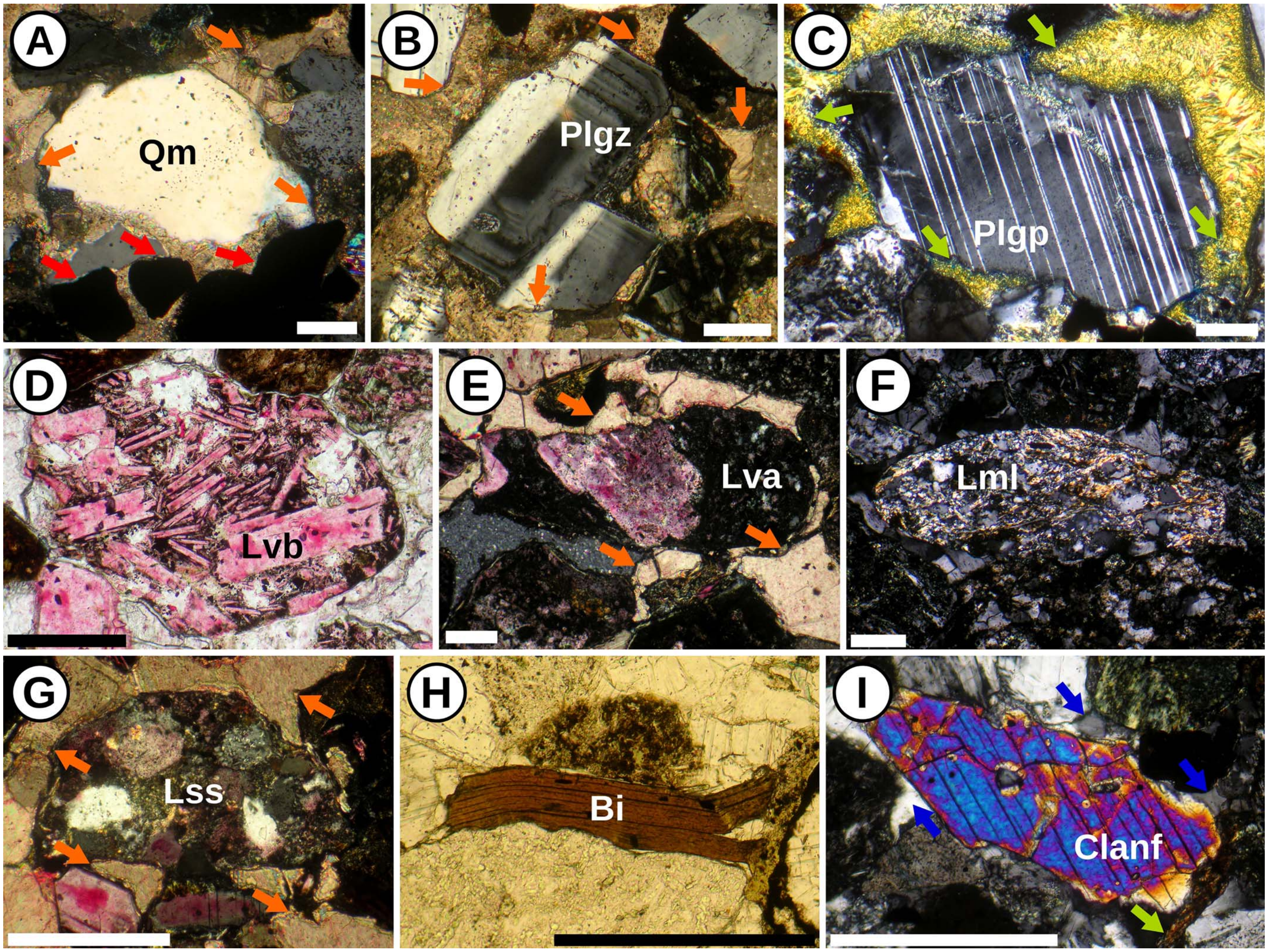

FIG. 4.—Photographs under a polarizing microscope for most representative grains recognized in the sandstone samples. **A)** Monocrystalline quartz fragment (Qm). **B)** Zoning plagioclase (Plgz). **C)** Polysynthetic twin plagioclase (Plgp). **D)** Lathwork texture with plagioclase microliths of a mafic volcanic lithic fragment (Lvb). **E)** Porphyritic texture from a felsic lithic volcanic fragment (Lva) with plagioclase phenocrystals immersed in a felsitic paste. **F)** Low-grade-metamorphic lithic fragment (Lml). **G)** Sandstone lithic fragment (Lss). **H)** Biotite accessory fragment (Bi). **I)** Amphibole accessory fragment (Clanf). Red, orange, green, and blue arrows highlight undifferentiated opaque mineral fragments, carbonate cement, clay–mineral cement, and zeolite cement, respectively. Scale bar on all photomicrographs measures 0.1 mm.

tuffaceous volcanic (Ltu, Fig. 5H), and felsic plutonic (Lpa, Fig. 5I). For conglomerate classification we follow the proposal of Limarino et al. (1996; in Scasso and Limarino 1997). Four sandstone samples (CBs-4$^{*}_{**}$, RCs-1$^{*}_{**}$, PJs-14$^{*}_{**}$ and RCs-II$^{*}_{**}$, respectively) correspond to the matrix of four conglomerate samples (i.e., CBc-4, RCc-1, PJc-13, and RCc-II) to allow comparison of their matrix and clastic-framework provenance signatures.

RESULTS

Sandstone Petrography, Classification, and Provenance

Sandstone samples of the Neogene succession (n = 62; see Appendix A) are mainly clast supported (59 samples), while only three are matrix-supported following the proposal of Dott (modified by Pettijohn et al. 1987). The grain size of detrital components varies between fine- to coarse-grained sand, and exceptionally some grains are coarser, reaching pebble and granule grain size. In general, textures are moderately sorted, and grains are subrounded to subangular.

Petrographic analysis allows us to recognize four main grain components, in decreasing order of abundance: rock fragments, feldspars, monocrystalline quartz, and polycrystalline quartz. Cements are represented mostly by calcium carbonate, clay, and zeolites. Optical porosity reaches a mean value of 0.8% (see Appendix A). Detrital composition and recalculation of ternary plots are also detailed in Appendix A.

Detrital Components.—The most abundant detrital components are lithic fragments (~ 70% on average), followed by total feldspars (18% on average), and quartz fragments (~ 6% on average). Volcanic grains are the most abundant of the lithic fragments (~ 60% on average) followed by metamorphic (~ 5% on average), plutonic (~ 2% on average), and sedimentary fragments (< 1% on average). Plagioclase feldspars are more abundant (~ 14% on average) than potassium feldspars (~ 4% on average). Monocrystalline quartz is the most abundant quartz type (~ 6% on average), while polycrystalline quartz is scarce (< 1% on average). For further data the reader is referred to Appendix A.

Accessory fragments are present in all samples with an average proportion of ~ 5%. We identify clinopyroxene, clinoamphibole, muscovite, and biotite, together with several grains of biological origin such as oyster fragments, bryozoans, and echinoderm plates. Clinopyroxenes are the most abundant

Downloaded from http://pubs.geoscienceworld.org/sepm/jsedres/article-pdf/95/4/760/7321069/10.2110_jsr.2024.005.pdf
by Universidad Nacional de La Plata user

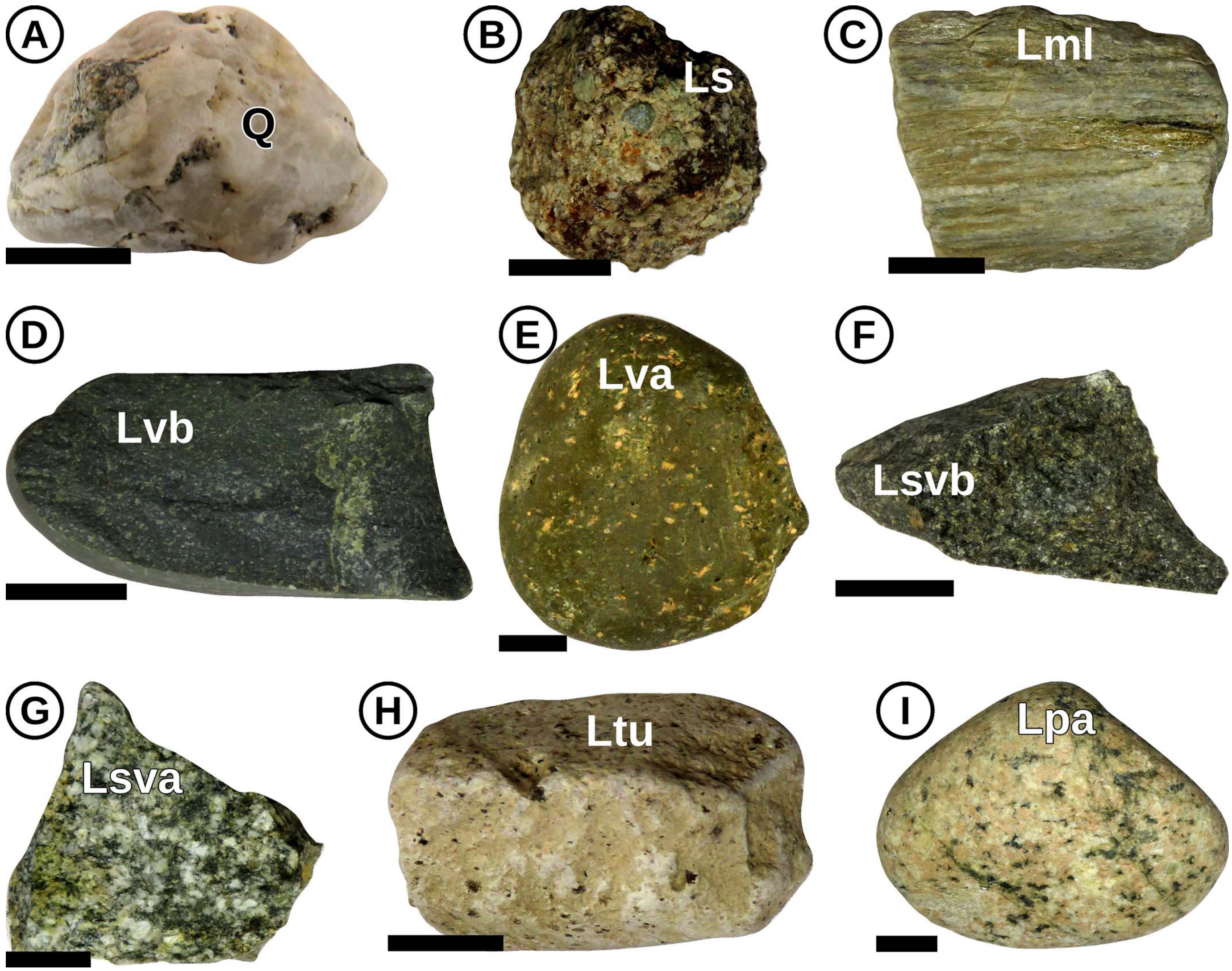

FIG. 5.—Conglomerate clasts types. **A)** Quartz fragment (Q). **B)** Sedimentary lithic fragment (Ls). **C)** Low-grade-metamorphic lithic fragment (Lml). **D)** Mafic volcanic lithic fragment (Lvb). **E)** Acid volcanic lithic fragment (Lva). **F)** Mafic subvolcanic lithic fragment (Lsvb). **G)** Acid subvolcanic lithic fragment (Lsva). **H)** Tuffaceous lithic fragment (Ltu). **I)** Acid plutonic lithic fragment (Lpa). Black scale bar measures 1 cm.

followed by opaque minerals. Biological grains were described and counted but were excluded for the provenance ternary diagrams. Accessory minerals present in high proportion were observed as complementary information for the provenance analysis of sandstone samples.

Cements.—Clay cement is dominant in sandstones of the study succession (Fig. 4). It consists of clay coatings where primary porosity is preserved. Commonly, clay cement completely occludes the pore space. Carbonate cement is present as calcite in some sandstones. Where it is present, this cement is dominant. It is composed of sparite that completely closes the pore space, though locally it consists of microsparite. Zeolitic cement appears as a coarse mosaic that completely occludes the pores between the sand-size grains. It is recognized as low-birefringence crystals of irregular shape that grow in the pores.

Classification.—The detrital composition of the study sandstones is homogeneous, with a high proportion of lithic fragments (see Appendix A). The average ratio of lithics to feldspars is 3:1, and the percentage of quartz is low, not exceeding $\sim$ 7% on average. The results obtained from the Gazzi-Dickinson point-counting method (Ingersoll et al. 1984) of the sandstones show that most of the samples are classified as litharenites and some are feldspathic litharenites of Folk et al. (1970) (for details the reader is remitted to Appendix A). The analyzed sediment samples show a low mineralogical maturity indicated by the high proportion of lithic and accessory fragments (mainly clinoamphibole and clinopyroxene) and scarcity of quartz grains. This maturity increases slightly towards the top of the study successions, evidenced by an increase in quartz content from $\sim$ 4% near the base to $\sim$ 28% at the top. Notably, the highest mineralogical maturity is observed in a sample from the lower bed of the SU-I of the LP section, decreasing markedly upwards in the overlying SU-II samples. The ratio of lithic fragments to feldspars remains relatively constant, both temporally and among the analyzed sections. In the LP section, the proportion of lithic fragments in the sandstones increases slightly from SU-I to SU-II.

Provenance.—In order to establish the provenance for the study area, modal-composition data from samples were plotted in the ternary diagram proposed by Dickinson et al. (1983) (Fig. 6A). Due to the slight variation in the composition of sandstones, ternary diagrams (Lm-Lv-Ls, Qm-Lvb-Lva,

Downloaded from http://pubs.geoscienceworld.org/sepm/jsedres/article-pdf/95/4/760/7321069/10.2110_jsr.2024.005.pdf
by Universidad Nacional de La Plata user

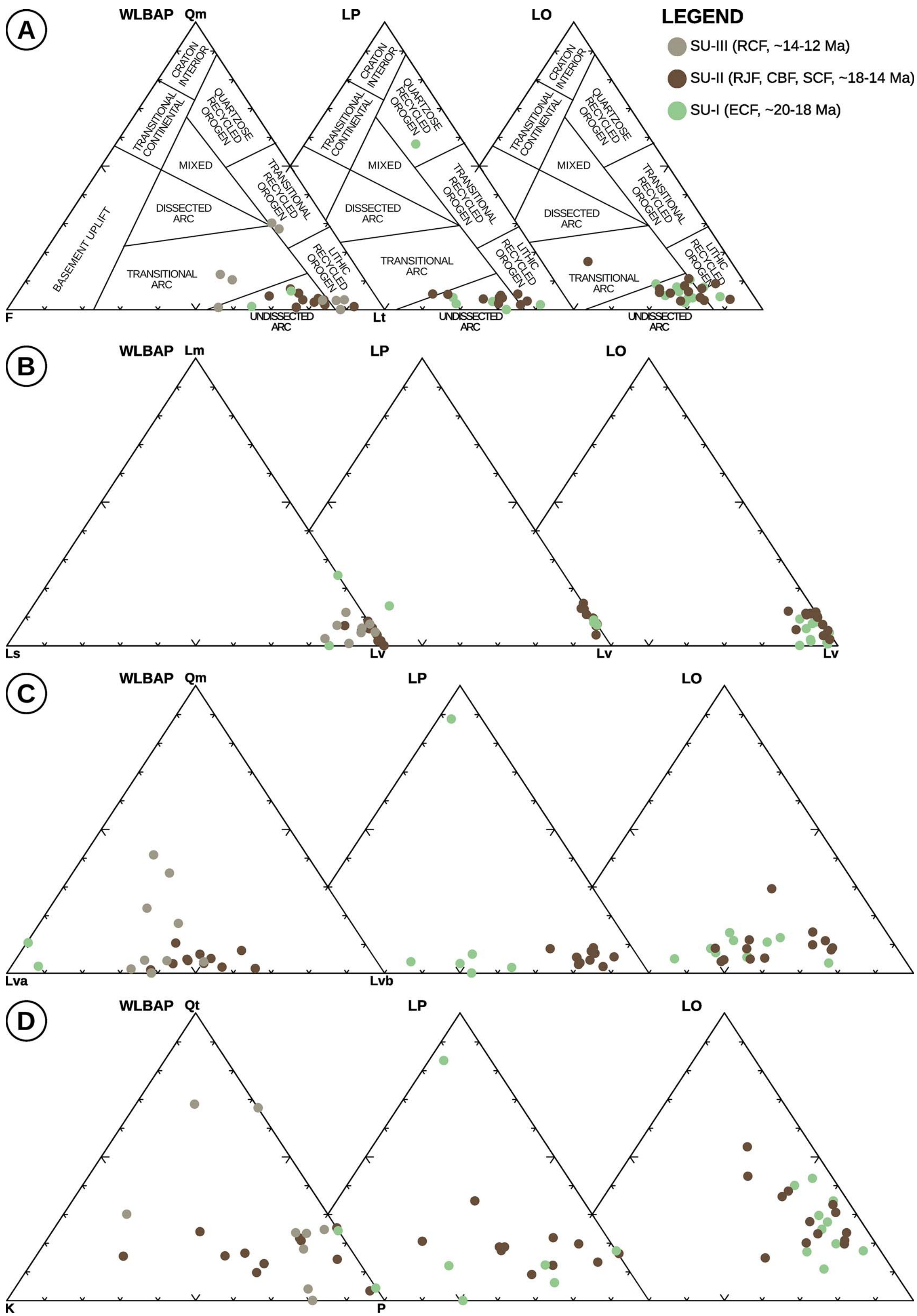

FIG. 6.—Sandstone ternary plots for tectonic and compositional discrimination for each stratigraphic section. Sedimentary units (SU) highlighted. **A)** Tectonic discrimination diagram proposed by Dickinson et al. (1983). Most samples are grouped in the lithic apex and classified mainly as magmatic arc and some in recycled orogen. Mean value for each section is highlighted and are clustered at undissected arc field. Qm, monocrystalline quartz fragments; F, total feldspar grains; Lt, total lithics and polycrystalline quartz fragments. **B)** Lm-Ls-Lv ternary diagram showing de predominance of Lv lithic fragments. Ls, total sedimentary lithic fragments; Lm, total metamorphic lithic fragments; Lv, total volcanic lithic fragments. **C)** Qm-Lva-Lvb ternary plot showing the variable proportion of mafic volcanic fragments and felsic volcanic fragments. Qm, monocrystalline quartz fragments; Lva, felsic volcanic fragments; Lvb, mafic volcanic fragments. **D)** Qt-P-K ternary diagram showing the variable proportion of potassium feldspar and total plagioclase fragments. Qt, total quartz grains; K, potassium feldspar grains; P, total-plagioclase fragments.

Downloaded from http://pubs.geoscienceworld.org/sepm/jsedres/article-pdf/95/4/760/7321069/10.2110_jsr.2024.005.pdf
by Universidad Nacional de La Plata user

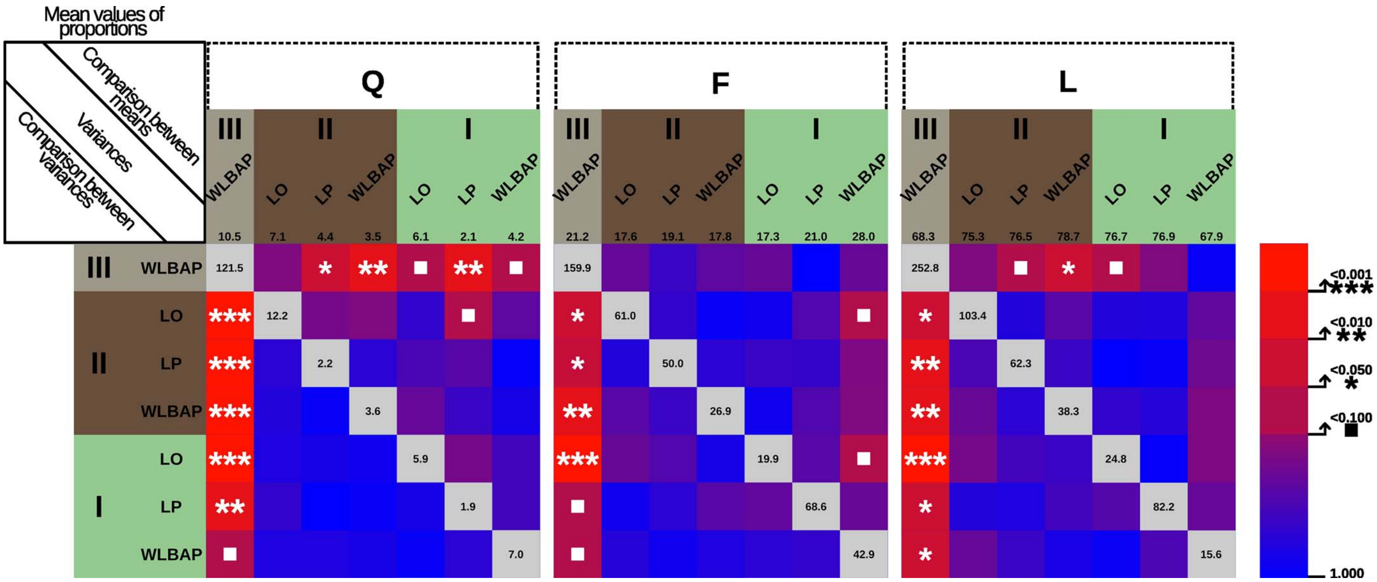

FIG. 7.—Pairwise comparisons of means (above the diagonal) and variances (below the diagonal) for the proportions of each grain type across statistical levels defined by the combination of section (WLBAP, LO, LP) and sedimentary unit (SU-I, SU-II, SU-III). The main diagonal displays variance values for each statistical level, while the mean proportions for each statistical level are indicated at the top of each box. The color gradient within each cell represents the p-value of the difference, with the significance thresholds as follows: *** for $p < 0.001$, ** for $p < 0.01$, * for $p < 0.05$, and ■ for $p < 0.1$. Q, quartz; F, feldspar; L, lithic. See Supplemental Appendix D for additional details.

and Qt-P-K; see Figs. 6B–D) were devised for the particularities of the study case, in order to better disperse the data and to understand spatio-temporal variations in sandstone composition.

Samples plotted in the Qm-F-Lt diagram of Dickinson et al. (1983) show that the majority (68%) are located in the undissected magmatic arc field, with another significant proportion (21%) falling in the recycled-orogen field (Fig. 6A). Around 90% of the study samples are located in magmatic-arc fields, of which ~ 68% belong to the undissected-arc field, and less than 1% of them to the transitional-arc field. Of the remaining ~ 32% of the samples, ~ 21% belong to lithic recycled orogen, ~ 11% to transitional recycled orogen and less than 1% (i.e., one sample) is plotted in the quartz-rich recycled-orogen field (Fig. 6A). The few samples that are located in the transitional and quartz-rich recycled-orogen fields have a proportion of quartz higher than 30%. They coincide with the base of SU-I of the LP section and SU-III of the WLBAP section. The average value of the sandstones corresponds to the ratio Qm_6:F_{19}:Lt_{75}, lying in the undissected-magmatic-arc field (Fig. 6A). Exploring temporal variations between SU-I and SU-II/SU-III, a slight shift from a lithic recycled orogen to an undissected arc is recognized (see below). It is noteworthy that in SU-II and SU-III an upward shift can be observed from the lithic-recycled orogen and magmatic-arc field to transitional recycled orogen and transitional magmatic arc, respectively.

Since lithic particles are dominant in the study succession, the Lm-Lv-Ls diagram aims to emphasize the discrimination among the population of lithic fragments, including total metamorphic (Lm), total volcanic (Lv), and total sedimentary (Ls) (Fig. 6B). This diagram gives a clear signal that the dominant fragments from most of the samples are volcanic, with an average ratio of Lm_7:Lv_{90}:Ls_3. This is consistent with a source area represented by an active volcanic arc without exposing orogenic roots, contributing material to the foreland area. This is particularly illustrated by the high proportion of Lv over Lm grains (Dickinson and Suczek 1979; Marsaglia and Ingersoll 1992).

The Qm-Lvb-Lva diagram with an average proportion of Qm_9:Lvb_{53}:Lva_{38}, shows a greater dispersion of samples and allowed discrimination of two spatial and temporal tendencies between marine and continental deposits: i) northern evolution (i.e., WLBAP) and ii) southern evolution (i.e., LP and LO sections) (Fig. 6C). In general, SU-I and the basal part of SU-II, have low proportions of quartz (Qm) and variable proportions of felsic (Lva) and mafic volcanic lithics (Lvb) (Fig. 6C). Comparing north-to-south trends for SU-I deposits, Lva fragments predominate in the north, while the proportion of Lva and Lvb fragments remains similar in the south (Fig. 6C). On the other hand, Lvb fragments dominate over Lva fragments in the southern SU-II beds. Meanwhile, the northern continental deposits (i.e., SU-II and SU-III) display an equal proportion of Lvb and Lva fragments. In both northern and southern sections there is an increase in the proportion of Qm towards the top of the sequence.

The Qt-P-K ternary plot with an average proportion of Qt_{24}:P_{59}:K_{17} shows that the northern and southern SU-I deposits are grouped separately, while the SU-II and SU-III form a single grouping (Fig. 6D). In general, SU-I has a higher proportion of plagioclase (P) over quartz (Qt) and K-feldspars (K) (Fig. 6D). In SU-I, samples from the northern sector lack K and present variable proportions of Qt. In contrast, samples from the southern sector show variable amounts of K and P. In southern sections, the LO stratigraphic section has a higher amount of Qt than the LP profile (Fig. 6D). Although the continental SU-II and SU-III present variable amounts of the three components, the dominance of P over K is notable and displays an increase in the proportion of Qt towards the younger units (Fig. 6D).

Based on the statistical analysis of the proportions of Q-F-L, SU-III at WLBAP shows the highest quartz proportions, showing strong support for differences compared to SU-II both at WLBAP and LP, moderate support compared to SU-I at LP, and weak support compared to SU-I either at WLBAP and LO (Fig. 7). In parallel, SU-III at WLBAP has the lowest lithic proportions, with moderate support for differences compared to SU-II at WLBAP and weak support compared to SU-II at LP and SU-I at LO (Fig. 7). Feldspar proportions were slightly higher in WLBAP SU-I compared to other levels (Fig. 7). However, these comparisons with LO SU-I and LO SU-II showed weak statistical support for differences with LO SU-I and LO SU-II, or no evidence, or weak statistical support for differences (Fig. 7).

Regarding variability, WLBAP SU-III exhibited the greatest variation among the three main grain types and was the only level with statistically significant differences in variance (Fig. 7). Comparisons of quartz variance show very strong support for differences in most cases, except for WLBAP

Downloaded from http://pubs.geoscienceworld.org/sepm/jsedres/article-pdf/95/4/760/7321069/10.2110_jsr.2024.005.pdf
by Universidad Nacional de La Plata user

SU-I, where weak support is likely due to a smaller sample size (Fig. 7). Differences in feldspar variance are most notable when comparing WLBAP SU-III to LO SU-I (very strong support), followed by WLBAP SU-II (strong support) and LP SU-II (moderate support), while the remaining comparisons show weak or no support. Variance in lithic grains for WLBAP SU-III mirrors the pattern observed for feldspar fragments, with very strong support for differences with LO SU-I, strong support for WLBAP SU-II and LP SU-II, and moderate support for the other comparisons. It is important to note that the comparative study and Figure 7 were carried out excluding sample CHs-1, as it is considered an outlier.

To summarize, between 20 and 18 Ma (SU-I) the sandstone samples provenance are marked with a lithic recycled orogen and undissected arc. In the overlying SU-II (~ 18–14 Ma), supply of sandstone samples is from an undissected arc with subordinate transitional arc and lithic recycled orogen. Finally, in SU-III (~ 14–12 Ma) sandstone sample provenance is from lithic and transitional recycled orogen and transitional arc.

Conglomerate Composition, Classification, and Provenance

Composition of Framework Clasts.—Quartz fragments are the only monomineralic component in the study samples. The average proportion is 9% and it is absent in only one sample (see Appendix B). This clast type is characterized by white to grayish-white color, low to moderate sphericity, and well to moderate roundness. These clasts are mainly homogeneous in composition (more than 95% of quartz), some other clasts of this category are associated with micaceous minerals (85% of quartz, 15% micaceous minerals).

Lithic fragments are the most abundant, exceeding 92% of the total clast counting, reaching 100% in one sample. Volcanic lithic fragments are the most abundant, with an average of 44%. In these fragments, Lvb and Lva were discriminated. Lva are the most abundant, with an average proportion of 37%. They are characterized by porphyritic textures with phenocrysts of feldspar and quartz immersed in a white, pale pink to pink-gray groundmass. They are well rounded and have moderate to high sphericity. The Lvb fragments occur with an average of 6%, showing black to gray-black colored with aphanitic texture. The shape is mostly oblate and moderately to highly rounded.

The tuffaceous lithic fragments (Ltu) follow Lv in abundance with an average proportion of 28% (Appendix B). They have an aphanitic texture with few phenocrystals of mafic minerals and quartz. The predominant color is white and light gray with pinkish tones. They show moderate degree of rounding and low to high sphericity.

The metamorphic lithics average 11% of counted clasts (Lml, Appendix B). They display a low degree of metamorphism and have a schistose texture. They are green-gray to blue-gray, oblate, of low sphericity, and of low to moderate degree of rounding.

The identified subvolcanic lithics are found in an average proportion of ~ 6% (Appendix B). They are subdivided according to their composition into mafic (Lsvb) and felsic subvolcanic lithics (Lsva). This category is characterized by a mix of porphyritic volcanic textures and very fine granular textures in the same fragments. In the subvolcanic lithic fragments, the Lsvb are the most abundant, having average proportions close to 4%. They are black to dark-gray with green tones, have a low degree of rounding, and low sphericity, and their typical shape is oblate. Meanwhile, the Lsva are found in an average proportion of around 2% (Appendix B). They are white to grayish-white in color, with low sphericity and a low degree of rounding.

The Lpa and Ls fragments are the scarcest of the clast types and are absent in three samples. Lpa (2% on average) are characterized by a pale pink color, fine to medium granular texture with quartz, feldspar, and mica crystals. They are well rounded and spherical. Ls fragments (1% on average) show clast-supported fabric, yellowish-brown colored, moderately spherical, and low degree of roundness.

Matrix Composition.—All the study conglomerate samples have sandy matrix with various fabrics. From base to top of the Río Correntoso Formation, samples change from a clast-supported to matrix-supported fabric (Aramendía et al. 2019). Although not well marked, there is an upward increase in quartz proportion. The maximum quartz peak is recorded in sample RCc-1.

Classification.—The six conglomerate samples were classified following the proposed of Limarino et al. (1996, in Scasso and Limarino 1997) (for a figure of this classification the reader is referred to Appendix B), taking into account the matrix, the fabric, and the composition of the framework clasts. Four samples were classified as lithic clast-supported orthoconglomerates, while the remaining two samples were classified as lithic matrix-supported orthoconglomerates. Although there are no marked temporal trends, a change in conglomerate fabric from base (i.e., clast-supported) to top (i.e., matrix-supported) is observed.

Provenance.—Compositionally, we record an increase in the proportion of quartz from a complete lack to ~ 34% in the conglomerates of SU-III, with the maximum quartz peak recorded in the youngest sample. When comparing these results with their corresponding sandy-matrix samples (see Methodology), they show a similar compositional trend. From a provenance point of view, conglomerate and sandstone samples display a similar evolution. The provenance is from an undissected magmatic-arc with a slightly upwards sequence increase of quartz fragments suggesting exposure of orogenic roots in the source area (for a figure of conglomerates provenance the reader is referred to Appendix B).

Mudstones Mineralogy Through X-Ray Diffraction

Non-Clay Minerals.—The analyzed samples comprise quartz (characteristic d-spacing of 3.34 Å and 4.26 Å), plagioclase (d-spacing of 3.21–3.22 Å), and K-feldspar (d-spacing of 3.18–3.21 Å) as the main detrital components. In addition, in some specific cases we observe high proportions of low-Mg calcite (d-spacing 3.03 Å), laumontite zeolite (d-spacing 9.01–9.12 Å), and gypsum (d-spacing 7.58 Å). A clay-mineral peak in the whole rock has a d-spacing between 14.65 and 16 Å but is further analyzed in clay-mineral diffractograms (see below).

The main identified non-clay minerals are, in order of decreasing abundance: quartz (~ 8% on average), plagioclase (~ 8% on average), and K-feldspar (~ 7% on average) (see Appendix C). Low-Mg calcite is also present in some levels (~ 4% on average). Laumontite is present only in WLBAP and LP sections (~ 2% on average), while subordinate amounts of gypsum are present only in the WLBAP section (< 1% on average).

Clay Minerals.—Smectite is the dominant clay mineral throughout the entire analyzed succession, varying between 40 and 100% (> 80% on average) (Appendix C). Smectite has, in general, sharp and symmetrical peaks between 12.3 and 14.1 Å on air-dried samples which expanded to ~ 17 Å following ethylene-glycol solvation, and collapsed to 9.81 Å following heating to 550°C. Also, smectite has well-defined reflections, and the absence of reflection in the glycolated sample between 6 and 9 Å (Fig. 8) shows that smectite is well crystallized and that in some samples it lacks illite interlayers. In some cases, smectite has wide asymmetric peaks, indicating that it is poorly crystallized or interstratified with illite.

Chlorite amounts vary between 0 and ~ 50% (12% on average) (Appendix C). It was determined by a series of basal reflections at 14.2, 7.26, and 3.54 Å that show no change upon glycol saturation and heating at 550°C (Fig. 8).

Illite is one of the less frequent clay minerals in the study succession (~ 6% on average). Nevertheless, the proportion of this mineral can reach

Downloaded from http://pubs.geoscienceworld.org/sepm/jsedres/article-pdf/95/4/760/7321069/10.2110_jsr.2024.005.pdf
by Universidad Nacional de La Plata user

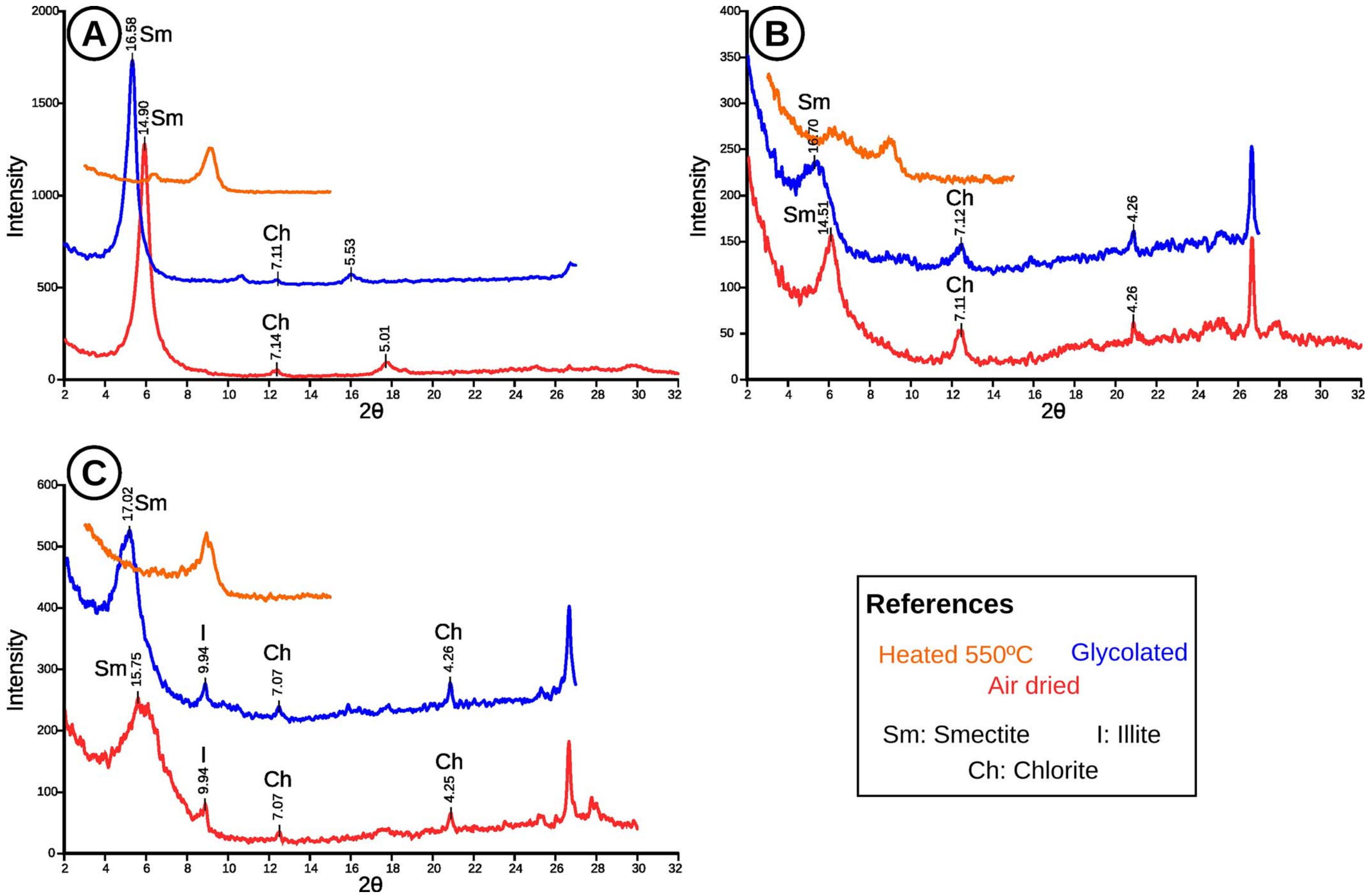

FIG. 8.—Diffractograms of clay minerals of Miocene sequence for the area. **A)** Clay minerals showing chlorite and well-crystallized smectite. **B)** Clay-mineral diffractogram showing chlorite accompanied with moderately crystallized smectite. **C)** Diffractogram showing illite, chlorite, and moderately to poorly crystallized smectite.

up to 35% in some levels (Appendix C). Illite is characterized by reflections at 10.06, 5.00, and 3.35 Å, and by the lack of change of the 10.06 Å peak upon glycol saturation. Crystallinity of illite is difficult to determine due to its scarcity in the analyzed samples.

Mixed-layers of illite–smectite (I/S) are present only by ~ 1% on average of the analyzed samples, reaching maximum values of 10% (Appendix C). Their XRD patterns are characterized by irregular and serrated peaks with variable basal reflections between 11.97 and 10.57 Å.

DISCUSSION

Sediment Source Areas for the Miocene Foreland Basin

Changes in sandstone composition and conglomerate lithic associations identified in the study sections are consistent with a shift of volcanic source areas during the Miocene (Fig. 9). The distribution of sedimentary units, paleocurrent data, and detrital-zircon maximum depositional ages previously reported by Cuitiño et al. (2015, 2019a) and Aramendía et al. (2019; 2022) are revised to compare the source areas identified.

The Miocene sedimentary record of the Austral–Magallanes basin is characterized by an overall regressive pattern, with an initial shallow marine sedimentation stage that grades transitionally upward to a continental environment (Cuitiño et al. 2015, 2019a, 2019b; Ghiglione et al. 2016; Aramendía et al. 2019, 2022). This scenario has been related to the synchronous Andean uplift, active volcanism near the subduction zone, progressive eastward migration of the deformation front, and the northward migration of the Chile Spreading Ridge (Ghiglione et al. 2016; Cuitiño et al. 2019a; Aramendía et al. 2019, 2022). The sedimentary deposits under study are located in the foreland zone near the cratonic area, which remains undeformed according to the model of DeCelles and Giles (1996). This is significant because the lack of deformation or eastward thrusting in the study area, combined with the eastward paleocurrent trends documented in previous studies (Cuitiño et al. 2019a; Aramendía et al. 2019, 2022), indicates sediment transport from the Southern Patagonian Andes (SPA) towards the basin, which served as the sediment sink during that period. Another notable feature of the study area, in contrast to the southern and southeastern region of the same basin, is the relatively thin Paleogene and Cretaceous sedimentary units available as sediment sources (Panza et al. 2001; Giacosa et al. 2001; Escosteguy et al. 2017). In contrast, Jurassic volcanic and volcaniclastic deposits, such as the El Quemado Complex, are extensive in both area and thickness.

According to the Qm-F-Lt ternary plot (Dickinson et al. 1983), the Miocene marine-basin infill of SU-I shows a general sediment source from an undissected magmatic arc (Figs. 6A, 9). This signature indicates sourcing from an active magmatic arc with no orogenic roots exposed. However, some volcanic grains may be recycled from older, widespread volcanic and volcaniclastic rocks such as those of the Jurassic El Quemado Complex, which forms the basin substrate. Compared with the U–Pb detrital-zircon ages, SU-I is characterized by Paleogene (e.g., the backarc Posadas Basalt and synchronous volcanism) zircon contributions, reflecting reworking of younger basin units typical of early foreland-basin cycles (*sensu* Allen and Allen 2005), along with consistent Early and Late Cretaceous (e.g., Río Tarde and Divisadero formations) peaks from older arc sources. Based on sandstone modal compositions, the continental beds of SU-II and SU-III have a subtle

Downloaded from http://pubs.geoscienceworld.org/sepm/jsedres/article-pdf/95/4/760/7321069/10.2110_jsr.2024.005.pdf
by Universidad Nacional de La Plata user

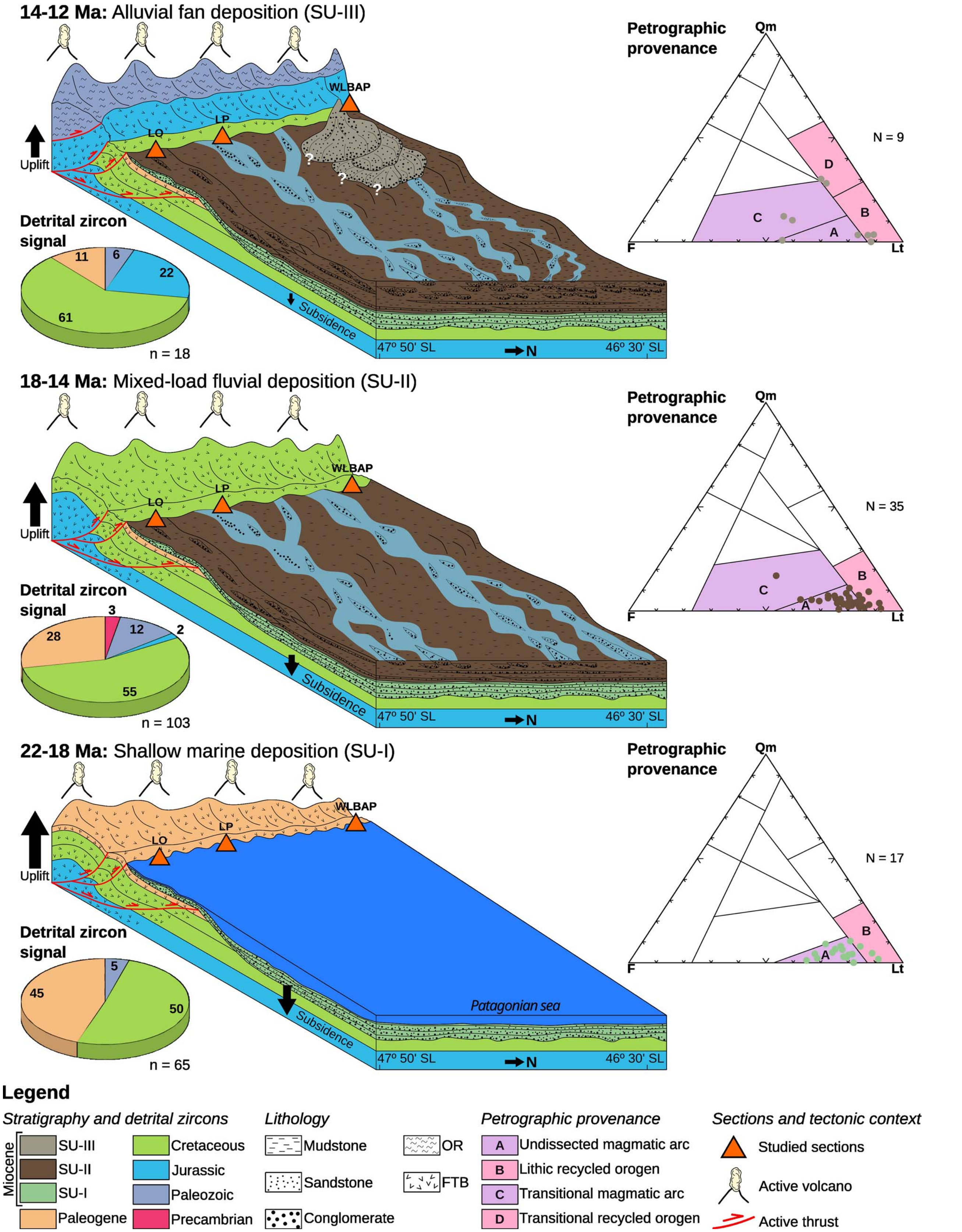

FIG. 9.—Integrated tectonostratigraphic provenance evolution for the study Miocene foreland basin infill describing an unroofing sequence for the area combining previous published detrital-zircon ages from Aramendía et al. (2022) and sandstone provenance associated with related conglomerate and mudstone samples. n, number of zircon grains; N, number of sandstone samples; FBT, fold and thrust belt; OR, orogenic roots.

Downloaded from http://pubs.geoscienceworld.org/sepm/jsedres/article-pdf/95/4/760/7321069/10.2110_jsr.2024.005.pdf
by Universidad Nacional de La Plata user

upward provenance variation. This includes an evolution from an undissected magmatic arc (similar to SU-I) to a transitional magmatic arc, and finally to a lithic recycled orogen (Figs. 6A, 9). These changes are expressed mostly as an upward increase first in feldspar proportion and later in quartz proportion. When compared with that of SU-I, the detrital-zircon ages for the SU-II show a decline in Paleogene and Late Cretaceous zircons, with a constant input of Early Cretaceous grains and an emerging upward contribution from Jurassic-aged rocks. Paleozoic and Precambrian sources are also in very small proportions (Fig. 9). Finally, the younger SU-III zircon population features increased Jurassic (e.g., El Quemado Complex and Ibáñez Formation) and Cretaceous input and not much input of Paleozoic grains, consistent with an unroofing sequence. Similar Andean orogenic unroofing processes were also observed in southern areas of the Austral–Magallanes Basin near Río Turbio and Cancha Carrera (Sickmann et al. 2019; Leonard et al. 2020), suggesting that this was a regional process.

The general sandstone-provenance evolution shows slight variations comparing the northern and southern sectors of the study zone (Figs. 6C, D, 9). The SU-I in the north (section WLBAP) shows a higher contribution of felsic volcanic fragments and dominance of plagioclase over K-feldspar. On the other hand, SU-I in the south (i.e., at LP and LO sections) shows equal proportions of mafic and felsic volcanic lithic fragments, while plagioclase and K-feldspar are in variable proportion. Despite these subtle differences, the fragments described indicate provenance from volcanic rocks. In SU-III at the WLBAP section, we identify the same compositional evolution in sandstones and their associated conglomerate beds, indicated by the parallel upward increase in quartz-rich fragments for both lithologies. A comparison between the north and south of the study area shows an upward increase in the amount of labile mafic volcanic lithic fragments over silicic lithic fragments, which could indicate that younger source areas (i.e., the Eocene Posadas Basalt or synchronous volcanism) may have been under erosion (Fig. 9) (Critelli and Criniti 2021). The absence of Miocene magmatic units in the study area is notable compared to the southern Austral–Magallanes Basin, where numerous Miocene plutonic bodies, such as the Fitz Roy and Torres del Paine plutons, are documented (Hervé et al. 2007; Sánchez-Valenzuela et al. 2021). Although these rocks are not preserved now, they likely existed and are evidenced only by the detrital zircons in the study area but were eroded due to Andean uplift, subsequent glaciations, and increased erosion.

The combined provenance data based on sandstone modal compositions and zircon U-Pb analysis can be explained using the unroofing sequence model proposed by Aramendía et al. (2022). This phenomenon is a product of sustained erosion of an uplifted orogenic chain and could be the cause of the removal of those hypothetical units. Unroofing could lead to a biased compositional interpretation of the source area assigned to the outcropping volcaniclastic Jurassic and metamorphic basement units. Although quartz grains may come from the disintegration of rhyolites, the parallel up-section increase of quartz and metamorphic lithic fragments suggests that these particles are associated with erosion of the orogenic roots, i.e., the older metamorphic rocks of the Río Lácteo Formation (in the Argentinean sector) and the Eastern Andean Metamorphic Complex (in the Chilean sector).

The main provenance from an undissected magmatic arc in the area may be related to sediment recycling from the underlying volcanic and sedimentary units exposed in the SPA to the west of the depocenter. The gradual, albeit subtle, but also the statistically strong to very strong support for p-values variances and mean values, and the increase in quartz towards the top of the succession, recorded only in SU-III, sustained in the statistical variance of Q and the relative loss of more labile fragments (i.e., lithics, accessories, among others) could mean a slight change in source rocks contributing sediments. On the one hand, this can be associated with an upward-increasing contribution from older units (e.g., metamorphic basement) because of an increase in the weathering rate of the orogen (i.e., source areas) (Johnsson 1993; Cox et al. 1995), or a sufficient time lapse at a constant weathering rate culminating in the exposure of the orogenic roots. Another trend observed in the ternary diagrams, also supported by statistical analysis, is the variation in the content of F fragments, which increases from SU-I to SU-III in detriment of the L fragments. Thermochronological data (Ronda et al. 2022) suggest that exhumation of the hinterland of the SPA was five times larger than that of the eastern slope of the SPA and took place between 20 and 10 Ma, partly supporting our hypothesis. Although the magnitude of weathering processes could have been different on each side of the orogen, this is a good approach to the magnitude of exposed units.

Environmental Controls on Clay Minerals

Clay minerals of the studied units have a very high proportion of smectite with well- to moderately crystallized structures (Fig. 8). Well-crystallized smectite can be interpreted as detrital, with no evidence of neoformation. On the other hand, moderately crystallized smectite suggests a minor influence of neoformation through the transformation of small amounts of illite (i.e., well-crystallized) to smectite, supported by the presence of low-Mg calcite. Low-Mg calcite indicates high ionic activity of Mg^{2+} in the pore solution. The Mg^{2+} cation interacts with illite and alters it to smectite (Watts 1980; Bouza et al. 2007). Detrital smectite forms mainly through the alteration of volcanic fragments, and we speculate that the high volcanic and pyroclastic activity in the Andean range contributed to the large amounts of smectite in the study succession. This clay mineral is ubiquitous across the three stratigraphic sections, ruling out any significant influence of burial diagenesis on the clay mineral assemblages (Raigemborn et al. 2014). Smectite tends to disappear in sedimentary basins that reach a medium grade of diagenesis (Pollastro 1993; Merriman and Peacor 1998; Raigemborn et al. 2014). Together with the scarcity of I/S, this suggests that the analyzed units were affected only by early diagenesis during burial (i.e., eodiagenesis) (Varela et al. 2013). The origins of the I/S mixed layers could be a result of moderate chemical weathering under surficial conditions (Chamley 1989). They may also form due to pedogenic processes under seasonal climates (Wilson 1999; Gonçalves et al. 2006; Raucsik and Varga 2008; Raigemborn et al. 2014) or through alteration of volcanic material (Lindgreen and Surlyk 2000; Net et al. 2002; Shoval 2004; Rostási et al. 2011).

Illite and chlorite are clay minerals commonly associated with smectite. Illite typically forms during the initial stages of chemical weathering in the source area under cool to temperate or dry conditions and under low-hydrolyzing weathering regimes (Nesbitt and Young 1984; Thiry 2000; Raigemborn et al. 2014). Chlorite, on the other hand, forms through the alteration and dissolution of volcaniclastic grains and Fe-Mg-rich minerals under low-hydrolyzing conditions in cool to temperate or dry climates (Nesbitt and Young 1984; Thiry 2000).

Illite and chlorite are associated with slightly pedogenized fine-grained facies of the three stratigraphic sections, suggesting an authigenic origin (Wilson 1999; Galán 2006; Gonçalves et al. 2006). The lack of detrital illite and chlorite in the analyzed samples is in accordance with the highly hydrolyzing conditions of the source area during the Miocene (Cravero et al. 2012).

The abundance of volcanic lithic fragments in the study succession, combined with their chemical weathering under conditions of slightly alkaline pH, high silica activity, and the presence of alkaline cations in solution, likely favored the formation of the described clay minerals (e.g., Burns and Ethridge 1979; Senkayi et al. 1987; McKinley et al. 2003; Raigemborn et al. 2014). These conditions facilitated the transformation of volcanic glass into smectite through hydration and the formation of zeolites, such as laumontite, as a secondary byproduct of this reaction (e.g., Williams and Crerar 1985; Senkayi et al. 1987; Arslan et al. 2010). Smectite-rich samples have also been documented in Miocene units farther south and along the coastal areas of the Austral–Magallanes Basin. This abundance is closely linked to the alteration of volcanic and volcaniclastic material in a warm, seasonal climate with intermittent cooling phases, as evidenced by the presence of illite, chlorite, and illite–smectite mixed layers (Matheos and Raigemborn 2012).

Downloaded from http://pubs.geoscienceworld.org/sepm/jsedres/article-pdf/95/4/760/7321069/10.2110_jsr.2024.005.pdf
by Universidad Nacional de La Plata user

Provenance Model

Allen and Allen (2005) describe the sedimentary evolution of a foreland basin through an unroofing sequence, outlining two logical steps: i) sediment is initially derived from units close in age to the uplift event, because these are the rocks most readily available for erosion, and ii) as older rocks are progressively exposed, they begin contributing to the sedimentary record, ultimately reaching the basement (i.e., orogenic roots). Critelli and Criniti (2021) offer a similar framework, focusing on sandstone petrography in ancient foreland basins. Their model proposes three sandstone types: i) quartz-rich sandstones sourced from the flanks of the lower plate, ii) variable provenance from the fold-and-thrust belt, reflecting an unroofing sequence, and iii) a predictable evolution characterized by an increase in feldspar and lithic fragments from older units, exposing the orogenic roots.

While both models aim to explain how sedimentation progresses to ultimately reveal orogenic roots (i.e., the oldest rocks) in a foreland basin, a key distinction lies in the type of orogeny they reference. Allen and Allen (2005) base their model on an Andean-type foreland basin, where an oceanic plate subducts beneath a continental plate. In contrast, Critelli and Criniti (2021) focus on collisional orogens, where two continental plates converge. This difference is significant, because the nature of the mountains associated with these foreland basins influences the lithologies exposed. Continent–continent collisions can yield a more varied lithology in terms of age and composition, whereas Andean-type orogens typically have a simpler evolution, with sediment sourced from a single continental plate dominated mainly by volcanic and volcaniclastic rocks derived from a magmatic arc due to collision of oceanic and continental plates.

In our study we analyze the provenance evolution of sandstones alongside conglomerates and mudstones, comparing these data with previously published detrital-zircon ages. Our results show that sandstones evolve from a dominance of lithic fragments sourced from an undissected magmatic arc and recycled orogenic lithics in SU-I (20–18 Ma), to an increase in feldspar proportions, indicating a transition from an undissected to a transitional magmatic arc in SU-II (18–14 Ma). Finally, SU-III (14–12 Ma) is characterized by increased quartz content and similar proportions of feldspar and lithic fragments, reflecting a transitional magmatic arc to a transitional recycled orogen.

The detrital-zircon record aligns with this progression, showing erosion beginning with Paleogene and Cretaceous units and culminating in a significant Jurassic contribution. Comparing these results with the two models, and considering the type of basin under study, the Allen and Allen (2005) model provides the best fit for both sandstone and detrital-zircon data in this region.

In accordance with the detrital-zircon ages documented in Aramendía et al. (2022), changes in sandstone and conglomerate provenance areas coincide with an unroofing sequence, in which the progressive upward enrichment of basement-derived particles is a consequence of progressive exposure of the orogenic roots during orogenic Miocene Andean uplift. Thermochronological data support a high-magnitude exhumation of the SPA during the Miocene, supporting the idea of a scenario of a rapid exposure of orogenic roots (Ronda et al. 2022).

CONCLUSIONS

The Miocene sedimentary evolution of the Austral–Magallanes Basin illustrates an unroofing sequence driven by Andean uplift, active volcanism, and eastward migration of the deformation front. Provenance analysis reveals a transition from lithic fragments of an undissected magmatic arc in SU-I (20–18 Ma) to increased feldspar contributions in SU-II (18–14 Ma) and, finally, quartz enrichment and recycled orogen inputs in SU-III (14–12 Ma). Detrital-zircon ages indicate sediment sources from Jurassic and older units, consistent with progressive erosion exposing orogenic roots, while variations in lithic associations across sections reflect differing source areas and erosion rates influenced by the magnitude of Southern Patagonian Andes exhumation. The studied units are dominated by smectite, mainly of detrital origin associated with the alteration of volcanic fragments, with minor neoformation linked to the transformation from illite that also creates mixed layers of illite–smectite. Scarce amounts of illite and chlorite, present in slightly pedogenized facies, suggest an authigenic origin associated with high hydrolyzing conditions and intermediate to felsic provenance during the Miocene. These clay minerals are also associated with calcite and laumontite. These mineral association reflect chemical weathering of volcanic lithics under slightly alkaline conditions with high silica and cation activity.

This sedimentary progression aligns with the Allen and Allen (2005) unroofing model, supported by detrital-zircon and thermochronological data, as well as paleocurrent trends and stratigraphic architecture. The northwestern margin of the basin exhibits a regressive pattern transitioning from shallow marine to continental environments, shaped by Andean tectonics and active volcanism. Thermochronological evidence highlights rapid exposure of orogenic roots during the Miocene, underscoring a straightforward sedimentary evolution dominated by contributions from a single continental-plate source, distinct from the more complex scenarios proposed by Critelli and Criniti (2021).

ACKNOWLEDGMENTS

We are grateful to technicians at X–ray diffraction lab, L. Vigiani and Germán Kürten, who were of great help for the measurements and diffractogram interpretation. We especially appreciated people who helped during fieldwork and contributed during subsequent discussions: R. Suárez, J. Ventisky, S. Vizcaíno, S. Bargo, G. Ronda, M. Ramos, and J. Tobal. We would like to thank Romain Voucher, who kindly helped to improve the final version; also the reviewers, Stephen Dobbs and Zachary Sickmann, and the associate editor, Devon Orme, for their valuable observations on the manuscript and figures, which greatly helped to enhance the paper. This work was carried out with the financial support of the research projects PICT 2015–0792 of the Agencia Nacional de Promoción Científica y Técnica, CONICET (PIP 11220200100307CO), UBA (UBACYT) and Agencia Nacional de Promoción Científica y Tecnológica (PICT–2020–SERIEA–03277).

REFERENCES

Aguirre-Urreta, M., and Ramos, V., 1981, Estratigrafía y paleontología de la alta cuenca de río Roble, provincia de Santa Cruz: Actas del 8° Congreso Geológico Argentino, Buenos Aires, Argentina, v. 3, p. 101–138.

Allen, P.A., and Allen, J.R., 2005, Basin Analysis: Principles and Application to Petroleum Play Assessment: John Wiley & Sons, 645 p.

Anderson, M.J., 2001, A new method for non-parametric multivariate analysis of variance: Austral Ecology, v. 26, p. 32–46, doi:10.1111/j.1442-9993.2001.01070.pp.x.

Anderson, M., and Braak, C.T., 2003, Permutation tests for multi-factorial analysis of variance: Journal of Statistical Computation and Simulation, v. 73, p. 85–113, doi:10.1080/00949650215733.

Aramendía, I., Ramos, M.E., Geuna, S., Cuitiño, J.I., and Ghiglione, M.C., 2018, A multidisciplinary study of the Lower Cretaceous marine to continental transition in the northern Austral–Magallanes basin and its geodynamic significance: Journal of South American Earth Sciences, v. 86, p. 54–69, doi:10.1016/j.jsames.2018.06.010.

Aramendía, I., Cuitiño, J.I., Ghiglione, M., and Bouza, P.J., 2019, Tectonostratigraphic significance of the Neogene sedimentary record of northwestern Austral–Magallanes Basin, Argentinean Patagonia: Latin American Journal of Sedimentology and Basin Analysis, v. 26, p. 99–126.

Aramendía, I., Cuitiño, J.I., Ghiglione, M.C., and Bouza, P.J., 2022, Timing and stratigraphic evolution of a Miocene foreland unroofing sequence in the Austral–Magallanes Basin during Southern Patagonian Andes uplift: Geological Society of London Journal, v. 180, p. jgs2022-038, doi:10.1144/jgs2022-038.

Arslan, M., Abdioğlu, E., and Kadir, S., 2010, Mineralogy, geochemistry, and origin of bentonite in Upper Cretaceous pyroclastic units of the Tirebolu Area, Giresun, northeast Turkey: Clays and Clay Minerals, v. 58, p. 120–141, doi:10.1346/CCMN.2010.0580112.

Barberón, V., Sue, C., Ghiglione, M., Ronda, G., and Aragón, E., 2018, Late Cenozoic brittle deformation in the Southern Patagonian Andes: record of plate coupling/decoupling during variable subduction?: Terra Nova, v. 30, p. 296–309, doi:10.1111/ter.12339.

Barberón, V., Ronda, G., Aramendía, I., Suárez, R.J., Ramos, M.E., Naipauer, M., Sue, C., and Ghiglione, M.C., 2019, Tectonic evolution of the northern Austral–Magallanes basin in the Southern Patagonian Andes from provenance analysis: Journal of South American Earth Sciences, v. 95, no. 102234, doi:10.1016/j.jsames.2019.102234.

Benjamin, D.J., Berger, J.O., Johannesson, M., Nosek, B.A., et al., 2017, Redefine statistical significance: Nature Human Behaviour, v. 2, p. 6–10, doi:10.1038/s41562-017-0189-z.

Downloaded from http://pubs.geoscienceworld.org/sepm/jsedres/article-pdf/95/4/760/7321069/10.2110_jsr.2024.005.pdf
by Universidad Nacional de La Plata user

Biscaye, P., 1965, Mineralogy and sedimentation of recent deep-sea clay in the Atlantic Ocean and Adjacent Seas and Oceans: Geological Society of America Bulletin, v. 76, p. 803–832, doi:10.1130/0016-7606(1965)76[803:MASORD]2.0.CO;2.

Blisniuk, P.M., Stern, L.A., Chamberlain, C.P., Idleman, B., and Zeitler, P.K., 2005, Climatic and ecologic changes during Miocene surface uplift in the Southern Patagonian Andes: Earth and Planetary Science Letters, v. 230, p. 125–142, doi:10.1016/j.epsl.2004.11.015.

Bouza, P.J., Simón, M., Aguilar, J., del Valle, H., and Rostagno, M., 2007, Fibrous-clay mineral formation and soil evolution in Aridisols of northeastern Patagonia, Argentina: Geoderma, v. 139, p. 38–50, doi:10.1016/j.geoderma.2007.01.001.

Bown, T.M., and Larriestra, C.N., 1990, Sedimentary paleoenvironments of fossil platyrrhine localities, Miocene Pinturas Formation, Santa Cruz Province, Argentina, *in* Fleagle, J.G., and Rosenberger, A.L., eds., The Platyrrhine Fossil Record: Academic Press, p. 87–119, doi:10.1016/B978-0-12-260345-7.50008-4.

Brown, G., and Brindley, G.W., 1980, X-ray diffraction procedures for clay mineral identification, *in* Brindley, G.W., and Brown, G., eds., Crystal Structures of Clay Minerals and their X-Ray Identification: Mineralogical Society of Great Britain and Ireland, v. 5, p. 305–059, doi:10.1180/mono-5.5.

Burns, L.K., and Ethridge, F.G., 1979, Petrology and diagenetic effects of lithic sandstones: Paleocene and Eocene Umpqua Formation southwest Oregon, *in* Sholle, P.A., and Schluger, P.R., eds., Aspects of Diagenesis: Society for Economic Paleontologists and Mineralogists, Special Publication 26, p. 307–317.

Caracciolo, L., Critelli, S., Innocenti, F., Kolios, N., and Manetti, P., 2011, Unravelling provenance from Eocene–Oligocene sandstones of the Thrace Basin, north-east Greece: Sedimentology, v. 58, p. 1988–2011, doi:10.1111/j.1365-3091.2011.01248.x.

Cavazza, W., 1989, Detrital modes and provenance of the Stilo-Capo d'Orlando Formation (Miocene), southern Italy: Sedimentology, v. 36, p. 1077–1090, doi:10.1111/j.1365-3091.1989.tb01543.x.

Chamley, H., 1989, Clay Sedimentology: Berlin, Springer, 223 p., doi:10.1007/978-3-642-85916-8.

Ciccioli, P.L., Marenssi, S.A., and Limarino, C.O., 2014, Petrology and provenance of the Toro Negro Formation (Neogene) of the Vinchina broken-foreland basin (Central Andes of Argentina): Journal of South American Earth Sciences, v. 49, p. 15–38, doi:10.1016/j.jsames.2013.10.003.

Collyer, M.L., and Adams, D.C., 2018, RRPP: an R package for fitting linear models to high-dimensional data using residual randomization: Methods in Ecology and Evolution, v. 9, p. 1772–1779, doi:10.1111/2041-210X.13029.

Collyer, M.L., and Adams, D., 2024, RRPP: Linear Model Evaluation with Randomized Residuals in a Permutation Procedure: R package version 2.1.0, https://CRAN.R-project.org/package=RRPP.

Collyer, M.L., Sekora, D.J., and Adams, D.C., 2015, A method for analysis of phenotypic change for phenotypes described by high-dimensional data: Heredity, v. 115, p. 357–365, doi:10.1038/hdy.2014.75.

Cox, R., Lowe, D.R., and Cullers, R.L., 1995, The influence of sediment recycling and basement composition on evolution of mudrock chemistry in the southwestern United States: Geochimica et Cosmochimica Acta, v. 59, p. 2919–2940, doi:10.1016/0016-7037(95)00185-9.

Cravero, F., Maiza, P.J., and Marfil, S.A., 2012, Halloysite in Argentinian deposits: origin and textural constraints: Clay Minerals, v. 47, p. 329–340, doi:10.1180/claymin.2012.047.3.04.

Critelli, S., and Criniti, S., 2021, Sandstone petrology and provenance in fold thrust belt and foreland basin system, *in* Al-Juboury, A., ed., Sedimentary Petrology: Implications in Petroleum Industry: Books on Demand, p. 1–15.

Critelli, S., and Ingersoll, R.V., 1995, Interpretation of neovolcanic versus palaeovolcanic sand grains: an example from Miocene deep-marine sandstone of the Topanga Group (southern California): Sedimentology, v. 42, p. 783–804, doi:10.1111/j.1365-3091.1995.tb00409.x.

Critelli, S., Le Pera, E., and Ingersoll, R.V., 1997, The effects of source lithology, transport, deposition and sampling scale on the composition of southern California sand: Sedimentology, v. 44, p. 653–671, doi:10.1046/j.1365-3091.1997.d01-42.x.

Critelli, S., Marsaglia, K.M., and Busby, C.J., 2002, Tectonic history of a Jurassic backarc-basin sequence (the Gran Cañon Formation, Cedros Island, Mexico), based on compositional modes of tuffaceous deposits: Geological Society of America, Bulletin, v. 114, p. 515–527, doi:10.1130/0016-7606(2002)114<0515:THOAJB>2.0.CO;2.

Cuitiño, J.I., Pimentel, M.M., Ventura Santos, R., and Scasso, R.A., 2012, High resolution isotopic ages for the early Miocene "Patagoniense" transgression in Southwest Patagonia: stratigraphic implications: Journal of South American Earth Sciences, v. 38, p. 110–122, doi:10.1016/j.jsames.2012.06.008.

Cuitiño, J.I., Ventura Santos, R., Alonso Muruaga, P.J., and Scasso, R.A., 2015, Sr-stratigraphy and sedimentary evolution of early Miocene marine foreland deposits in the northern Austral (Magallanes) Basin, Argentina: Andean Geology, v. 42, p. 364–385, doi:10.5027/andgeoV42n3-a05.

Cuitiño, J.I., Vizcaíno, S.F., Bargo, M.S., and Aramendía, I., 2019a, Sedimentology and fossil vertebrates of the Santa Cruz Formation (early Miocene) in Lago Posadas, southwestern Patagonia, Argentina: Andean Geology, v. 46, p. 383–420, doi:10.5027/andgeoV46n2-3128.

Cuitiño, J.I., Varela, A.N., Ghiglione, M.C., Richiano, S., and Poiré, D.G., 2019b, The Austral–Magallanes basin (southern Patagonia): a synthesis of its stratigraphy and evolution: Latin American Journal of Sedimentology and Basin Analysis, v. 26, p. 155–166.

De Barrio, R.E., Schillato-Yané, G., and Bond, M., 1984, La Formación Santa Cruz en el borde occidental del Macizo del Deseado (Provincia de Santa Cruz) y su contenido paleontológico: 9th Congreso Geológico Argentino, Actas, v. IV, p. 539–556.

DeCelles, P.G., and Giles, K.A., 1996, Foreland basin systems: Basin Research, v. 8, p. 105–123, doi:10.1046/j.1365-2117.1996.01491.x.

Dickinson, W.R., 1970, Interpreting detrital modes of graywacke and arkose: Journal of Sedimentary Petrology, v. 40, p. 695–707, doi:10.1306/74D72018-2B21-11D7-8648000102C1865D.

Dickinson, W.R., 1985, Interpreting provenance relations from detrital modes of sandstones, *in* Zuffa, G.G., ed., Provenance of Arenites: Dordrecht, Springer, p. 333–361, doi:10.1007/978-94-017-2809-6_15.

Dickinson, W.R., and Suczek, C.A., 1979, Plate tectonics and sandstone compositions: American Association of Petroleum Geologists, Bulletin, v. 63, p. 2164–2182.

Dickinson, W.R., Beard, L.S., Brakenridge, G.R., Erjavec, J.L., Ferguson, R.C., Inman, K.F., Knepp, R.A., Lindberg, F.A., and Ryberg, P.T., 1983, Provenance of North American Phanerozoic sandstones in relation to tectonic setting: Geological Society of America, Bulletin, v. 94, p. 222, doi:10.1130/0016-7606(1983)94<222:PONAPS>2.0.CO;2.

Dushoff, J., Kain, M.P., and Bolker, B.M., 2019, I can see clearly now: reinterpreting statistical significance: Methods in Ecology and Evolution, v. 10, p. 756–759, doi:10.1111/2041-210X.13159.

Encinas, A., Folguera, A., Riffo, R., Molina, P., Fernández Paz, L., Litvak, V.D., Colwyn, D.A., Valencia, V.A., and Carrasco, M., 2019, Cenozoic basin evolution of the Central Patagonian Andes: evidence from geochronology, stratigraphy, and geochemistry: Geoscience Frontiers, v. 10, p. 1139–1165, doi:10.1016/j.gsf.2018.07.004.

Escosteguy, L.D., Franchi, M., and Dal Molin, C., 2001, Formación Ligorio Márquez (Paleoceno superior–Eoceno inferior) en el río Zeballos, provincia de Santa Cruz, Argentina: 11° Congreso Latinoamericano de Geología, 3° Congreso Uruguayo de Geología, Montevideo.

Escosteguy, L.D., Dal Molin, C.N., Franchi, M., Geuna, S.E., and Lapido, O.R., 2003, Hoja Geológica 4772-II Lago Buenos Aires: Servicio Geológico Minero Argentino, Instituto de Geología y Recursos Minerales, https://repositorio.segemar.gov.ar//handle/308849217/148.

Escosteguy, L.D., Etcheverría, M.P., Geuna, S.E., Franchi, M., Wilson, C., Azcurra, D., and Panza, J.L.A., 2017, Hoja Geológica 4972-I Monte Tetris: Servicio Geológico Minero Argentino, Instituto de Geología y Recursos Minerales, https://repositorio.segemar.gov.ar//handle/308849217/2783.

Feruglio, E., 1949, Descripcion geologica de la Patagonia: Dirección General de Yacimientos Petrolíferos Fiscales, Buenos Aires, Argentina.

Folguera, A., Encinas, A., Echaurren, A., Gianni, G., Orts, D., Valencia, V., and Carrasco, G., 2018, Constraints on the Neogene growth of the central Patagonian Andes at the latitude of the Chile triple junction (45–47°S) using U/Pb geochronology in synorogenic strata: Tectonophysics, v. 744, p. 134–154, doi:10.1016/j.tecto.2018.06.011.

Folk, R.L., Andrews, P.B., and Lewis, D.W., 1970, Detrital sedimentary rock classification and nomenclature for use in New Zealand: New Zealand Journal of Geology and Geophysics, v. 13, p. 937–968, doi:10.1080/00288306.1970.10418211.

Fosdick, J.C., Grove, M., Hourigan, J.K., and Calderón, M., 2013, Retroarc deformation and exhumation near the end of the Andes, southern Patagonia: Earth and Planetary Science Letters, v. 361, p. 504–517, doi:10.1016/j.epsl.2012.12.007.

Furque, G., 1973, Descripción geológica de la Hoja 58b, Lago Argentino, provincia de Santa Cruz: Servicio Geológico Minero Argentino, Boletín 140, p. 1–49.

Galán, E., 2006, Genesis of clay minerals, *in* Bergaya, F., Theng, B.K.G., and Lagaly, G., eds., Developments in Clay Science: Elsevier, Handbook of Clay Science, v. 1, p. 1129–1162, doi:10.1016/S1572-4352(05)01042-1.

Garzanti, E., Doglioni, C., Vezzoli, G., and Andò, S., 2007, Orogenic belts and orogenic sediment provenance: The Journal of Geology, v. 115, p. 315–334, doi:10.1086/512755.

Ghiglione, M.C., Quinteros, J., Yagupsky, D., Bonillo-Martínez, P., Hlebszevtich, J., Ramos, V.A., Vergani, G., Figueroa, D., Quesada, S., and Zapata, T., 2010, Structure and tectonic history of the foreland basins of southernmost South America: Journal of South American Earth Sciences, v. 29, p. 262–277, doi:10.1016/j.jsames.2009.07.006.

Ghiglione, M.C., Naipauer, M., Sue, C., Barberón, V., Valencia, V., Aguirre-Urreta, B., and Ramos, V.A., 2015, U–Pb zircon ages from the northern Austral basin and their correlation with the Early Cretaceous exhumation and volcanism of Patagonia: Cretaceous Research, v. 55, p. 116–128, doi:10.1016/j.cretres.2015.02.006.

Ghiglione, M.C., Sue, C., Ramos, M.E., Tobal, J.E., and Gallardo, R.E., 2016, The relation between Neogene orogenic growth in the Southern Andes and sedimentation in the offshore Argentine and Malvinas basins during the opening of the Drake Passage, *in* Ghiglione, M.C., ed., Geodynamic Evolution of the Southernmost Andes Connections with the Scotia Arc: Springer International Publishing, p. 109–136.

Giacosa, R.E., Franchi, M., Genini, A., and Panza, J.L.A., 2001, Hojas Geológicas 4772-III Lago Belgrano y 4772-IV Lago Posadas: Servicio Geológico Minero Argentino, Instituto de Geología y Recursos Minerales, https://repositorio.segemar.gov.ar//handle/308849217/199.

Gonçalves, D.F., Rossetti, D.F., Truckenbrodt, W., and Mendes, A.C., 2006, Argilominerais da Formação Codó (Aptiano Superior), Bacia de Grajaú, nordeste do Brasil: Latin American Journal of Sedimentology and Basin Analysis, v. 13, p. 59–75.

Gorring, M.L., Kay, S.M., Zeitler, P.K., Ramos, V.A., Rubiolo, D., Fernandez, M.I., and Panza, J.L., 1997, Neogene Patagonian plateau lavas: continental magmas associated with ridge collision at the Chile Triple Junction: Tectonics, v. 16, p. 1–17, doi:10.1029/96TC03368.

Hervé, F., Pankhurst, R.J., Fanning, C.M., Calderón, M., and Yaxley, G.M., 2007, The South Patagonian batholith: 150 my of granite magmatism on a plate margin: Lithos, v. 97, p. 373–394, doi:10.1016/j.lithos.2007.01.007.

Downloaded from http://pubs.geoscienceworld.org/sepm/jsedres/article-pdf/95/4/760/7321069/10.2110_jsr.2024.005.pdf
by Universidad Nacional de La Plata user

Hervé, F., Calderón, M., and Faúndez, V., 2008, The metamorphic complexes of the Patagonian and Fuegian Andes: Geologica Acta, v. 6, p. 43–53.

Holm, S., 1979, A simple sequentially rejective multiple test procedure: Scandinavian Journal of Statistics, v. 6, p. 65–70.

Horton, B.K., 2018, Sedimentary record of Andean mountain building: Earth-Science Reviews, v. 178, p. 279–309, doi:10.1016/j.earscirev.2017.11.025.

Horton, B.K., Constenius, K.N., and DeCelles, P.G., 2004, Tectonic control on coarse-grained foreland-basin sequences: an example from the Cordilleran foreland basin, Utah: Geology, v. 32, p. 637, doi:10.1130/G20407.1.

Howard, J.L., 1993, The statistics of counting clasts in rudites: a review, with examples from the upper Palaeogene of southern California, USA: Sedimentology, v. 40, p. 157–174, doi:10.1111/j.1365-3091.1993.tb01759.x.

Hutchinson, C.S., 1974, Laboratory Handbook of Petrographic Techniques: New York, Wiley, 527 p.

Ingersoll, R.V., 1983, Petrofacies and provenance of late Mesozoic forearc basin, northern and central California: American Association of Petroleum Geologists, Bulletin, v. 67, p. 1125–1142, doi:10.1306/03B5B713-16D1-11D7-8645000102C1865D.

Ingersoll, R.V., 1990, Actualistic sandstone petrofacies: discriminating modern and ancient source rocks: Geology, v. 18, p. 733–736, doi:10.1130/0091-7613(1990)018<0733:ASPDMA>2.3.CO;2.

Ingersoll, R.V., Bullard, T.F., Ford, R.L., Grimm, J.P., Pickle, J.D., and Sares, S.W., 1984, The effect of grain size on detrital modes: a test of the Gazzi-Dickinson point-counting method: Journal of Sedimentary Petrology, v. 54, p. 103–116, doi:10.1306/212F83B9-2B24-11D7-8648000102C1865D.

Jervey, M.T., 1988, Quantitative geological modeling of siliciclastic rock sequences and their seismic expression, *in* Wilgus, C.K., Hastings, B.S., Posamentier, H., Van Wagoner, J., Ross, C.A., and Kendall, C.G.St.C, eds., Sea–Level Changes: An Integrated Approach: SEPM, Special Publication 42, p. 47–69.

Johnsson, M.J., 1993, The system controlling the composition of clastic sediments, *in* Johnsson, M.J., and Basu, A., eds., Processes Controlling the Composition of Clastic Sediments: Geological Society of America, p. 21–40, doi:10.1130/SPE284-p1.

Kay, S.M., Ramos, V., and Gorring, M.L., 2002, Geochemistry of Eocene plateau basalts related to ridge collision in Southern Patagonia, *in* XV Congreso Geologico Argentino (Calafate), Buenos Aires, Argentina, Actas: Asociación Geológica Argentina, v. 3, p. 60–65.

Kraemer, P.E., and Riccardi, A.C., 1997, Estratigrafía de la región comprendida entre los lagos Argentino y Viedma, Santa Cruz: Asociación Geológica Argentina, Revista, v. 52, p. 333–360.

Lagabrielle, Y., Suárez, M., Rossello, E.A., Hérail, G., Martinod, J., Régnier, M., and De La Cruz, R., 2004, Neogene to Quaternary tectonic evolution of the Patagonian Andes at the latitude of the Chile Triple Junction: Tectonophysics, v. 385, p. 211–241, doi:10.1016/j.tecto.2004.04.023.

Leonard, J.S., Fosdick, J.C., and VanderLeest, R.A., 2020, Erosional and tectonic evolution of a retroarc orogenic wedge as revealed by sedimentary provenance: case of the Oligocene–Miocene Patagonian Andes: Frontiers in Earth Science, v. 7, doi:10.3389/feart.2019.00353.

Lindgreen, H., and Surlyk, F., 2000, Upper Permian–Lower Cretaceous clay mineralogy of East Greenland: provenance, palaeoclimate and volcanicity: Clay Minerals, v. 35, p. 791–806, doi:10.1180/000985500547241.

Malumián, N., and Náñez, C., 2011, The Late Cretaceous–Cenozoic transgressions in Patagonia and the Fuegian Andes: foraminifera, palaeoecology, and palaeogeography: Biological Journal of the Linnean Society, v. 103, p. 269–288, doi:10.1111/j.1095-8312.2011.01649.x.

Marsaglia, K.M., and Ingersoll, R.V., 1992, Compositional trends in arc-related, deep-marine sand and sandstone: a reassessment of magmatic-arc provenance: Geological Society of America, Bulletin, v. 104, p. 1637–1649, doi:10.1130/0016-7606(1992)104<1637:CTIARD>2.3.CO;2.

Matheos, S.D., and Raigemborn, M.S., 2012, Sedimentology and paleoenvironment of the Santa Cruz Formation, *in* Vizcaino, S.F., Kay, R.F., and Bargo, S.M., eds., Early Miocene Paleobiology in Patagonia: High-Latitude Paleocommunities of the Santa Cruz Formation: Cambridge University Press, p. 59–82.

McKinley, G.A., Follows, M.J., Marshall, J., and Fan, S.M., 2003, Interannual variability of air–sea O_2 fluxes and the determination of CO_2 sinks using atmospheric O_2/N_2: Geophysical Research Letters, v. 30, p. 1101, doi:10.1029/2002GL016044.

Merriman, R.J., and Peacor, D.R., 1998, Very low-grade metapelites: mineralogy, microfabrics and measuring reaction progress, *in* Frey, M., and Robinson, D., eds., Low-Grade Metamorphism: John Wiley & Sons, p. 10–60, doi:10.1002/9781444313345.ch2.

Moore, D.M., and Reynolds, R.C., 1997, X-Ray Diffraction and the Identification and Analysis of Clay Minerals: Oxford, Oxford University Press, 400 p.

Nesbitt, H.W., and Young, G.M., 1984, Prediction of some weathering of basalts: American Journal of Science, v. 292, p. 740–770.

Net, L.I., Alonso, M.S., and Limarino, C.O., 2002, Source rock and environmental control on clay mineral associations, lower section of Paganzo Group (Carboniferous), northwest Argentina: Sedimentary Geology, v. 152, p. 183–199, doi:10.1016/S0037-0738(02)00068-4.

Panza, J.L.A., Cobos, J.C., Zubía, M.A., and Franchi, M., 2001, Hoja Geológica 4769-III Destacamento La María: Servicio Geológico Minero Argentino, Instituto de Geología y Recursos Minerales, Boletín 269, p. 84.

Parras, A., and Cuitiño, J.I., 2021, Revised chrono and lithostratigraphy for the Oligocene–Miocene Patagoniense marine deposits in Patagonia: implications for stratigraphic cycles, paleogeography, and major drivers: Journal of South American Earth Sciences, v. 110, p. 103327, doi:10.1016/j.jsames.2021.103327.

Parras, A., Dix, G.R., and Griffin, M., 2012, Sr-isotope chronostratigraphy of Paleogene–Neogene marine deposits: Austral Basin, southern Patagonia (Argentina): Journal of South American Earth Sciences, v. 37, p. 122–135, doi:10.1016/j.jsames.2012.02.007.

Pettijohn, F.J., Potter, P.E., and Siever, R., 1987, Sand and Sandstone: New York, Springer-Verlag, 553 p.

Pollastro, R.M., 1993, Considerations and applications of the illite/smectite geothermometer in hydrocarbon-bearing rocks of Miocene to Mississippian age: Clays and Clay Minerals, v. 41, p. 119–133, doi:10.1346/CCMN.1993.0410202.

Raigemborn, M.S., 2008, Estudio estratigráfico, sedimentológico y composicional de las sedimentitas del Terciario Inferior (Grupo Río Chico) en el sector sudoriental del Chubut Extraandino [Ph.D. Thesis]: Universidad Nacional de La Plata, p. 367 doi:10.35537/10915/4369.

Raigemborn, M.S., Gómez-Peral, L.E., Krause, J.M., and Matheos, S.D., 2014, Controls on clay minerals assemblages in an early Paleogene nonmarine succession: implications for the volcanic and paleoclimatic record of extra-Andean Patagonia, Argentina: Journal of South American Earth Sciences, v. 52, p. 1–23, doi:10.1016/j.jsames.2014.02.001.

Ramos, V.A., 1989, Andean foothills structures in northern Magallanes Basin, Argentina: American Association of Petroleum Geologists, Bulletin, v. 73, p. 887–903, doi:10.1306/44B4A28A-170A-11D7-8645000102C1865D.

Ramos, V.A., and Kay, S.M., 1992, Southern Patagonian plateau basalts and deformation: backarc testimony of ridge collisions: Tectonophysics, v. 205, p. 261–282, doi:10.1016/0040-1951(92)90430-E.

Raucsik, B., and Varga, A., 2008, Climato-environmental controls on clay mineralogy of the Hettangian–Bajocian successions of the Mecsek Mountains, Hungary: an evidence for extreme continental weathering during the early Toarcian oceanic anoxic event: Palaeogeography, Palaeoclimatology, Palaeoecology, v. 265, p. 1–13, doi:10.1016/j.palaeo.2008.02.004.

Richiano, S., Varela, A.N., Cereceda, A., and Poiré, D.G., 2012, Evolución paleoambiental de la Formación Río Mayer, Cretácico inferior, cuenca Austral, provincia de Santa Cruz, Argentina: Latin American Journal of Sedimentology and Basin Analysis, v. 19, p. 3–26.

Richiano, S., Varela, A.N., Gómez-Peral, L.E., Cereceda, A., and Poiré, D.G., 2015, Composition of the Lower Cretaceous source rock from the Austral Basin (Río Mayer Formation, Patagonia, Argentina): regional implication for unconventional reservoirs in the Southern Andes: Marine and Petroleum Geology, v. 66, p. 764–790, doi:10.1016/j.marpetgeo.2015.07.018.

Richiano, S., Varela, A.N., and Poiré, D.G., 2016, Heterogeneous distribution of trace fossils across initial transgressive deposits in rift basins: an example from the Springhill Formation, Argentina: Lethaia, v. 49, p. 524–539, doi:10.1111/let.12163.

Ronda, G., Ghiglione, M.C., Barberón, V., Coutand, I., and Tobal, J., 2019, Mesozoic–Cenozoic evolution of the Southern Patagonian Andes fold and thrust belt (47–48°S): influence of the Rocas Verdes basin inversion and onset of Patagonian glaciations: Tectonophysics, v. 765, p. 83–101, doi:10.1016/j.tecto.2019.05.009.

Ronda, G., Ghiglione, M.C., Martinod, J., Barberón, V., Ramos, M.E., Coutand, I., Grujic, D., and Kislitsyn, R., 2022, Early Cretaceous to Cenozoic growth of the Patagonian Andes as revealed by low-temperature thermochronology: Tectonics, v. 41, p. e2021TC007113, doi:10.1029/2021TC007113.

Rostási, Á., Raucsik, B., and Varga, A., 2011, Palaeoenvironmental controls on the clay mineralogy of Carnian sections from the Transdanubian Range (Hungary): Palaeogeography, Palaeoclimatology, Palaeoecology, v. 300, p. 101–112, doi:10.1016/j.palaeo.2010.12.013.

Sánchez-Valenzuela, A., de Saint Blanquat, M., Hervé, F., Polvé, M., Morata, D., de Parseval, P., and Benoit, B., 2021, Geochemistry of Cenozoic plutonic rocks in the extra-Andean southern Patagonia as evidence for a magmatic arc migration process: Andean Geology, v. 48, p. 359–402, doi:10.5027/andgeov48n3-3158.

Scalabrino, B., Lagabrielle, Y., Rupelle, A., de la, Malavieille, J., Polvé, M., Espinoza, F., Morata, D., and Suarez, M., 2009, Subduction of an Active Spreading Ridge Beneath Southern South America: A Review of the Cenozoic Geological Records from the Andean Foreland, Central Patagonia (46–47°S), *in* Lallemand, S., and Funiciello, F., eds., Subduction Zone Geodynamics: Berlin, Springer, p. 227–246, doi:10.1007/978-3-540-87974-9_12.

Scasso, R.A., and Limarino, C.O., 1997, Petrología y diagénesis de rocas clásticas: Buenos Aires, Asociación Argentina de Sedimentología, Publicación Especial, 258 p.

Schultz, L.G., 1964, Quantitative interpretation of mineralogical composition from X-ray and chemical data for the Pierre Shale: U.S. Geological Survey, Professional Paper 391-C, p. 1–31, doi:10.3133/pp391C.

Senkayi, A.L., Ming, D.W., Dixon, J.B., and Hossner, L.R., 1987, Kaolinite, opal-CT, and clinoptilolite in altered tuffs interbedded with lignite in the Jackson Group, Texas: Clays and Clay Minerals, v. 35, p. 281–290, doi:10.1346/CCMN.1987.0350405.

Shoval, S., 2004, Deposition of volcanogenic smectite along the southeastern Neo-Tethys margin during the oceanic convergence stage: Applied Clay Science, v. 24, p. 299–311, doi:10.1016/j.clay.2003.08.009.

Sickmann, Z.T., Schwartz, T.M., Malkowski, M.A., Dobbs, S.C., and Graham, S.A., 2019, Interpreting large detrital geochronology data sets in retroarc foreland basins: an example from the Magallanes–Austral Basin, southernmost Patagonia: Lithosphere, v. 11, p. 620–642, doi:10.1130/L1060.1.

Sinito, A.M., 1980, Edades geológicas, radimétricas y magnéticas de algunas vulcanitas cenozoicas de las provincias de Santa Cruz y Chubut: Asociación Geológica Argentina, Revista, v. 35, p. 332–339.

Downloaded from http://pubs.geoscienceworld.org/sepm/jsedres/article-pdf/95/4/760/7321069/10.2110_jsr.2024.005.pdf
by Universidad Nacional de La Plata user

Spalletti, L.A., Limarino, C.O., and Piñol, F.C., 2012, Petrology and geochemistry of Carboniferous siliciclastics from the Argentine Frontal Cordillera: a test of methods for interpreting provenance and tectonic setting: Journal of South American Earth Sciences, v. 36, p. 32–54, doi:10.1016/j.jsames.2011.11.002.

Suárez, M., 1976, Plate-tectonic model for southern Antarctic Peninsula and its relation to southern Andes: Geology, v. 4, p. 211–214, doi:10.1130/0091-7613(1976)4<211:PMFSAP>2.0.CO;2.

Thiry, M., 2000, Palaeoclimatic interpretation of clay minerals in marine deposits: an outlook from the continental origin: Earth-Science Reviews, v. 49, p. 201–221, doi:10.1016/S0012-8252(99)00054-9.

Thomson, S.N., Hervé, F., and Stöckhert, B., 2001, Mesozoic–Cenozoic denudation history of the Patagonian Andes (southern Chile) and its correlation to different subduction processes: Tectonics, v. 20, p. 693–711, doi:10.1029/2001TC900013.

Thomson, S.N., Brandon, M.T., Tomkin, J.H., Reiners, P.W., Vásquez, C., and Wilson, N.J., 2010, Glaciation as a destructive and constructive control on mountain building: Nature, v. 467, p. 313–317, doi:10.1038/nature09365.

Ton-That, T., Singer, B.S., Mörner, N.-A., and Rabassa, J., 1999, Datación de lavas basálticas por $^{40}Ar/^{39}Ar$ y geología glacial de la región del lago Buenos Aires, provincia de Santa Cruz, Argentina: Asociación Geológica Argentina, Revista, v. 54, p. 333–352.

Ugarte, F.R.E., 1956, El Grupo de Río Zeballos en el flanco occidental de la meseta Buenos Aires (provincia de Santa Cruz): Asociación Geológica Argentina, Revista, v. 11, p. 202–216.

Varela, A.N., Gómez-Peral, L.E., Richiano, S., and Poiré, D.G., 2013, Distinguishing similar volcanic source areas from an integrated provenance analysis: implications for foreland Andean basins: Journal of Sedimentary Research, v. 83, p. 258–276, doi:10.2110/jsr.2013.22.

Vaucher, R., Musajo, C., Spangenberg, J.E., Poyatos-Moré, M., Zeeden, C., Puigdefàbregas, C., Prieur, M., Castelltort, S., and Adatte, T., 2024, Sediment supply variation control on lower Eocene delta sequences (Tremp Basin, Spain): Geology, v. 53, p. 83–88, doi:10.1130/G52548.1.

Watts, N.L., 1980, Quaternary pedogenic calcretes from the Kalahari (southern Africa): mineralogy, genesis and diagenesis: Sedimentology, v. 27, p. 661–686, doi:10.1111/j.1365-3091.1980.tb01654.x.

Williams, L.A., and Crerar, D.A., 1985, Silica diagenesis; II, General mechanisms: Journal of Sedimentary Petrology, v. 55, p. 312–321, doi:10.1306/212F86B1-2B24-11D7-8648000102C1865D.

Wilson, M.J., 1999, The origin and formation of clay minerals in soils: past, present and future perspectives: Clay Minerals, v. 34, p. 7–25, doi:10.1180/000985599545957.

Received 8 January 2024; accepted 24 April 2025.

Downloaded from http://pubs.geoscienceworld.org/sepm/jsedres/article-pdf/95/4/760/7321069/10.2110_jsr.2024.005.pdf
by Universidad Nacional de La Plata user